School of Engineering and Information Technology

ENG460 – Engineering Thesis

(Quality Assessment in conductors)

Corrosion Detection in ACSR Cables

[55]

A report submitted to School of Engineering and Information Technology, Murdoch University in partial fulfilment of the requirements for the degree of Bachelor of Engineering

Nisar Jaffrey
Supervisor: Sujeewa Hettiwatte

2013

Abstract

Overhead transmission lines are the most economical and commonly used carriers of electricity. Aluminium Conductor Steel Reinforced (ACSR) cables, as part of transmission lines, are used in severe environments in coastal areas and industrial zones for many years. These cables are affected by galvanic corrosion in the interface between the aluminium and steel strands. On the other hand, it is important for power companies to use efficient technology to locate and repair any significant faults on transmission lines at the earliest possible stage that could help them reduce maintenance costs and increase the quality of the power supply. This report investigates the existing methods of corrosion detection used in ACSR cables of overhead transmission lines, and estimates the location of corrosion through simulation in a computer program. In particular, the report analyses two promising methods of corrosion detection, namely "electromagnetic induction" and "time domain reflectometry", and explains in detail their principle of operation and efficiency. In addition, the report also mentions some of the corrosion detectors available on the market and discusses their characteristics. In the latter part of the report, one of the existing techniques is thoroughly investigated by implementing in a computer program, and the simulation results are discussed. It also describes a few obstacles that might be faced if the technology is applied practically, and offers suggestions for a better approach to the problem.

Disclaimer

I declare the following to be my own work, unless otherwise referenced, as defined by the university's policy on plagiarism.

Signed: *Nisar Jaffrey*

Date: 18/11/2013

Acknowledgement

This project would not have been possible without the help of some great people with their extra ordinary assistance.

I would like to thank my supervisor Dr Sujeewa Hettiwatte for his guidance in this project and for offering his time to help me progress throughout.

I am also highly indebted to my parents who supported me interminably since I opened my eyes for the first time.

Last but not the least, I am very grateful to my wife Halima and the precious diamond of my life, Laraib for their support, patience and motivation.

Table of Contents

Abstract i
Disclaimer ii
Acknowledgement iii
List of Acronyms vi
List of Figures vii
List of Tables viii
Chapter 1: Introduction 1
1.1 Introduction 1
1.2 Aluminium Conductor Steel Reinforced (ACSR) Cables 2
1.3 Failure Mechanism in ACSR Cables 2
1.4 Objective of the Project 3
1.5 Scope of the Work 3
1.6 Literature Review 4
Chapter 2: Inspection Techniques 6
2.1 Existing Methods of Corrosion Detection 6
2.1.1 Non-Destructive Testing (NDT) 6
2.1.2 Magnetic Method 8
Chapter 3: Electromagnetic Induction Method 10
3.1 Electromagnetic Induction (Eddy Current Testing) 10
3.1.1 Principle of Operation: 10
3.2 Detectors Based on Eddy Current Technology Available in Market 15
3.2.1 Cormon OHLCD Technology 15
3.2.2 Fujikura's Detector 15
3.2.3 Detection Services offered by ATTAR in Australia 15
Chapter 4: Transmission Line 16
4.1 Transmission Line 16
4.2 Transmission Line Parameters 17
4.2.1 Series Resistance 17
4.2.2 Series Inductance 17
4.2.3 Shunt Capacitance 19
4.2.4 Shunt Conductance 20
4.3 Transmission Line Modelling 21

4.3.1 Distributed Parameter Line Model (Long Line Model) 21
Chapter 5: Time Domain Reflectometry 25
5.1 Time Domain Reflectometry 25
5.1.1 Principle of Operation 26
5.2 Reflection from Typical Load Terminations 27
5.2.1 Open Circuit Termination 28
5.2.2 Short Circuit Termination 28
5.2.3 Matched Impedance Termination 29
5.2.4 Complex Load Impedances 30
5.3 Transients in Transmission Tine TDR 32
5.3.1 The Bounce Diagram 33
5.4 Some Important Factors in TDR Analysis 36
5.4.1 Propagation Velocity 36
5.4.2 Calculation of Location of Mismatch Impedance 36
5.4.3 Characteristic Impedance 37
Chapter 6: Application of TDR in this Project 38
6.1 Calibration of TDR Measuring System 38
6.2 Modelling in SimPowerSystems Toolbox 40
6.3 Modelling Corrosion in the Cable 42
6.4 Confirmation of Appropriate Circuit Design 42
Chapter 7: Simulation Results and Discussion 44
7.1 Detection and Localization of Corrosion 44
7.2 Multiple Corrosions 50
Chapter 8: Conclusion and Future Recommendation 58
8.1 Conclusion 58
8.2 Future Work Recommendation 60
Appendices 61
Appendix A 61
Appendix B 63
Appendix C 64
Appendix D 65
References: 71

List of Acronyms

AC	Alternating Current
ACSR	Aluminium Conductor Steel Reinforced
DC	Direct Current
GMR	Geometric Mean Radius
NDT	Non Destructive Testing
SWR	Standing Wave Ratio
TDR	Time Domain Reflectometry

List of Figures

Figure 1: ACSR cable 2
Figure 2 Magnetic flux induced in a cable by permanent magnet 8
Figure 3: Principle of operation of eddy current testing method 11
Figure 4: Power transmission lines 16
Figure 5: Three phase line 18
Figure 6: Three-phase, two-conductor bundled line 19
Figure 7: Distributed parameter equivalent circuit 22
Figure 8: Equivalent π-model 24
Figure 9: Block diagram of a time domain reflectometer 26
Figure 10: Oscilloscope displays 26
Figure 11: Transmission and reflection coefficient 27
Figure 12: Typical load terminations and their respective waveforms 29
Figure 13: TDR display for complex loads 31
Figure 14: Transient on transmission line 32
Figure 15: Voltage bounce diagram 34
Figure 16: Voltage bounce diagram for the example under consideration 35
Figure 17: Three-phase bundled line used for TDR 38
Figure 18: Pulse movement along the transmission line 39
Figure 19: Block diagram for TDR analysis on transmission line 40
Figure 20 TDR result from matched load 43
Figure 21: Corrosion planted at 25km on the line 45
Figure 22: TDR Result for corrosion at 25 km 45
Figure 23: TDR Result for corrosion at 100 km 47
Figure 24: TDR Result for corrosion at 150 km 48
Figure 25: TDR Result for corrosion at 200 km 49
Figure 26: Corrosion at two points 50
Figure 27: TDR Result for multiple corrosion at two points 51
Figure 28: Multiple corrosion at three points 52
Figure 29: TDR Result for multiple corrosion at three points 53
Figure 30 : Multiple corrosion at four points 54
Figure 31: TDR Result for multiple corrosion at four points 55
Figure 32: Multiple corrosion at five points 56
Figure 33: TDR Result for multiple corrosion at five points 56
Figure 34: ACSR Cable specifications 63
Figure 35: Nominal π-model 64
Figure 36: Equivalent π-model 69

List of Tables

Table 1: Comparison of various types of NDT techniques [33] 14
Table 2: The overall TDR result for each single fault on the line 49
Table 3: TDR result for double faults on the line at two points 51
Table 4: TDR result for multiple faults on the line at three points 53
Table 5: TDR result for multiple faults on the line at four points 55
Table 6: TDR result for multiple faults on the line at five points 57

This page is intentionally blank

Chapter 1

- Introduction
- Aluminium Conductor Steel Reinforced (ACSR) cables
- Failure Mechanism in ACSR Cables
- Objective of the Project
- Scope of the Work
- Literature review

Chapter 1: Introduction

1.1 Introduction

Overhead power transmission lines usually run in severe environments for many years and therefore, the cables are exposed to harsh climatic variations such as wind, rain, pollution, etc. This leads to gradual degradation of the conductor and consequently to unexpected costly problems and poor power supply quality, if not dealt with in a timely fashion [46]. Aluminium conductor steel reinforced (ACSR) cables are the most commonly used conductors in overhead transmission lines. They are usually affected by galvanic corrosion, which is a key factor causing failure of the cable, and hence, refurbishment of the transmission line. A critical phase in this process is the loss of zinc from the galvanized steel strands because, once the galvanizing is lost, the aluminium strands get exposed to rapid galvanic corrosion.

On the other hand, consistency and reliability of electrical energy has become more important recently due to greater competition and restricted resources [40], and therefore, the need for sufficient technology for timely fault detection on transmission lines has significantly increased.

1.2 Aluminium Conductor Steel Reinforced (ACSR) Cables

Aluminium has substituted copper as the most frequently used conductor metal in overhead transmission lines due to its lower cost and lighter weight. Among different aluminium conductor types, Aluminium conductor steel reinforced (ACSR) cables, as shown in figure 1, are widely used in power delivery systems around the globe.

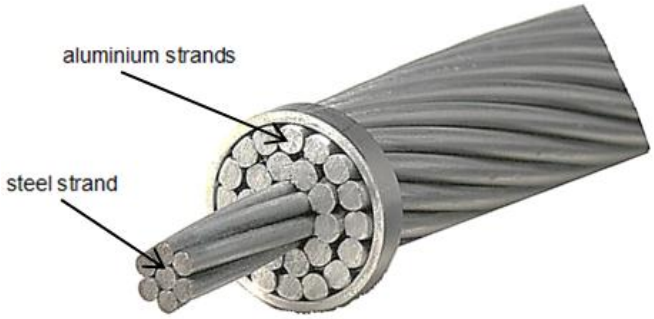

Figure 1: ACSR cable [56]

These cables comprise a solid or stranded steel core surrounded by one or more layers of aluminium wires. So far, the majority of these conductors have lasted 25-40 years and in some cases up to 50 years [32]. Therefore, long term exposure to severe environments means they require maintenance or refurbishment.

1.3 Failure Mechanism in ACSR Cables

In power transmission system the common failure mechanism limiting the life of ACSR cable is internal corrosion [51]. In ACSR cables the chance of galvanic corrosion between the steel core and the aluminium strands has been, since the beginning, understood and preventive methods such as coating of steel strands applied. Nevertheless, certain atmospheric factors such as industrial pollution or marine salts in the air may still cause serious corrosion [18].

One of the most deteriorating problems, besides mechanical fatigue, found on ACSR conductors is chemical corrosion. Unpleasant environments like industrial pollution or atmospheric marine salts can corrode the conductor externally, but this may not be as severe as internal corrosion, due to the fact that the cross-sectional loss of the

conductor is not usually ample in this case. On the other hand, the internal corrosion is a more serious problem, wherein the pollution and water vapour enter the edge between the steel and aluminium wires inside the cable [6].The corrosion of the steel strands in ACSR cables comes into effect as soon as the coated zinc disappears from the steel core wires, making the inner aluminium act anodic and hence prone to galvanic corrosion, leading to strand rupture [19]. When the cross-sectional area of the conductor shrinks due to such a rupture, initially, there is an increase in power flow in other aluminium strands, but then the flow enters the steel strands, which fast-tracks the occurrence of corrosion and significantly reduces the life of the cable [9].

1.4 Objective of the Project

The main purpose of this project is to evaluate the existing methods of corrosion detection used in ACSR cables, and to estimate the location of corrosion through simulation of a corroded cable in a computer program such as MATLAB. This needs to be done through overwhelming research on the topic that would lead to identification of the most appropriate method(s) to address the problem, and then implementing one of the techniques in a computer program to assess its feasibility and practicality.

1.5 Scope of the Work

The work undertaken throughout this project involves the following tasks:

- Detailed research on prevailing methods of corrosion detection;
- Description of the two most promising methods;
- Calculation of transmission line parameters;

- Selection of a random ACSR conductor for the purpose of investigation;
- Modelling transmission line, and hence modelling the chosen ACSR conductor;
- Modelling corrosion within the cable;
- Implementation and simulation in a computer program;
- Discussion of simulation results;
- Investigation of the outcome of the project;
- Suggestion for future work.

1.6 Literature Review

In 1991 Havard et al. [27] investigated Ontario Hydro's transmission lines and introduced a useful method for prediction of corrosion and failure assessment of transmission line conductors. Their extensive assessment proved that the loss of zinc from the galvanized steel core can be spotted by an overhead line corrosion detector, while an infrared camera might be able to detect any ruptured or corroded aluminium strands. The most important outcome was the modification of the corrosion detector for live line measurement of galvanized loss from the steel cores of the ACSR cable [27]. This inventive work is now broadly followed to estimate the residual life of the well-used conductors.

According to a research by Fisher et al. [13] in 1989, helicopter carried infrared sensors can be used to investigate aluminium corrosion in transmission lines with severe deterioration and extremely corroded strands, but this method is not suitable for early damage detection.

The literature by Sutton et al. [51] in 1986 mentions that an electromagnetic method was developed at Central Electricity Research Laboratories (CERL), in Leatherhead, (UK) that could detect galvanizing loss in ACSR cables. In this method, eddy currents are induced around the strands of the conductor as soon as high frequency currents are excited through a winding in the sensor head. These eddy

currents produce magnetic flux which is sensitive to strand corrosion and can be detected on a portable unit.

In their work, Baltazar et al. [3] in 2010, studied the propagation of guided waves in ACSR cable for structural damage detection using time–frequency analysis based on short time Fourier transform. The outcome indicated that mechanical contact among the wires produces mode conversion of longitudinal to flexural modes. The monitoring of these flexural modes proved to be useful in detection of corrosion in conductors.

A non-destructive testing method has been designed in the literature [37] which is able to detect the location and severity of corrosion of steel rebar and strands. This method utilizes time domain reflectometry. By using a sensor wire beside steel reinforcement, a transmission line is formed. If there exists any flaw in the steel reinforcement, it will alter the electromagnetic properties of the transmission line. The results of both analytical model and laboratory assessment have proved that TDR can be successfully operated to detect, localize and classify the extent of damage in steel reinforcement by this method.

The literature by Wang et al. [54] investigates the theory of time domain reflectometry TDR and frequency domain reflectometry, and then introduces joint time-frequency domain reflectometry for diagnosis of power cables.

Chapter 2

- Existing Methods of Corrosion Detection
- Non-Destructive Testing (NDT)
- Magnetic method

Chapter 2: Inspection Techniques

2.1 Existing Methods of Corrosion Detection

The corrosion of aluminium and steel strands in ACSR cables is one of the primary causes of stability problems that affect ageing transmission lines. A reliable and cost-effective technique for detection, localization, and measuring the degree of loss can lead to improved levels of power supply quality, and may benefit the power companies by decreasing maintenance costs through early detection. In order to do so, the testing methods should permit inspection of material without damaging its prospect usefulness [40]. Non-destructive testing (NDT) is a suitable approach to fulfil this condition.

2.1.1 Non-Destructive Testing (NDT)

NDT is a technique in material science that conducts testing and scrutinizing objects without causing any destruction to them [40]. In electrical engineering, NDT has been used for detection, characterization, localization and sizing of discontinuities [40]. A number of NDT techniques have been introduced to detect and locate flaws in power transmission lines using various methods such as:

- Visual inspection;
- Infrared camera inspection;

- Ultrasonic inspection;
- Neutron Radiography;
- Magnetic method;
- Electromagnetic induction (eddy current);
- Time Domain Reflectometry.

It is worth mentioning that the majority of these methods need mobilisation by foot, ground vehicle, or air vehicle, and require labour presence in the locality of the line. Traditionally, the most commonly used technique of fault detection has been the visual inspection method [37]. However, it cannot be used to detect internal corrosion in conductors.

Helicopter carried infrared sensors can be used to investigate aluminium corrosion in transmission lines with severe deterioration and extremely corroded strands but is not suitable for early damage detection [13].

The principles of operation of some of the above listed techniques are explained below.

2.1.2 Magnetic Method

In ACSR, the steel strands play a supportive role for aluminium, and hence detection of any corroded strand of steel core is an important practice to assure safety and quality in power supply process [30]. The Magnetic method of corrosion detection requires the test object to be a ferromagnetic material [33] like steel that can be magnetized. Detection sensors based on this theory for corroded steel strands in ACSR have been developed which are carried by inspection robots to inspect conductors along transmission lines [30, 7].

Principle of Operation:

As shown in figure 2, the steel strands in ACSR are magnetized by a permanent magnet and sensor coils that give a voltage proportional to the induced magnetic flux. The permanent magnet saturates longitudinally a segment *"l"* of the conductor.

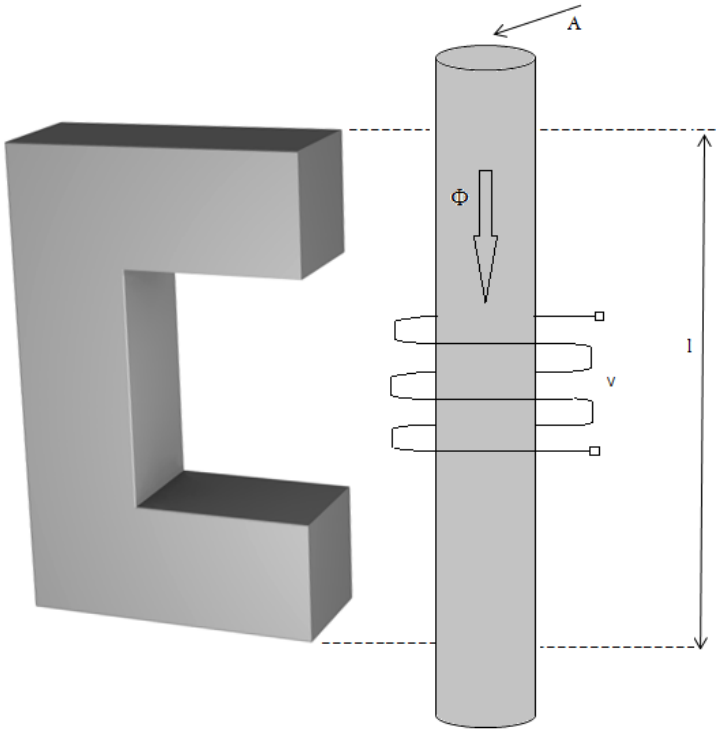

Figure 2: Magnetic flux induced in a cable by permanent magnet [7]

From Faraday's law of induction, the change in the magnetic field around the coil induces a voltage, V, given by:

$$\mathrm{V} = -N\frac{d\Phi}{dt} \qquad ---------- (1)$$

Where *N* is the number of turns of coil;

Φ is the magnetic flux;

The induced magnetic flux is then given by:

$$\Phi = \int \mathrm{B}.d\mathrm{A} \qquad ---------- (2)$$

Where,

B is magnetic flux density;

$d\mathrm{A}$ is the area element vector;

The longitudinal flux is proportional to the area of cross-section of the conductor when it gets magnetically saturated [7].

That is:

$$\Phi = \mathrm{B}.\mathrm{A} \qquad ---------- (3)$$

Where, *A* is the area covered by *B.*

Substituting equation (3) in equation (1)

$$\mathrm{V} = -\mathrm{N}.\mathrm{B}.\frac{\mathrm{dA}}{\mathrm{dt}} \qquad ---------- (4)$$

Here, *N* and *B* are constants; hence, this equation shows that any change in the voltage of the coil measures the change of area *A*. In other words, a spotted change in V corresponds to change in *A,* which can be used to discover any flaws in the conductor.

In following chapters, the two important detection techniques are discussed in detail.

Chapter 3

- Electromagnetic Induction (Eddy Current Testing)
- Detectors based on eddy current technology available in market

---

Chapter 3: Electromagnetic Induction Method

3.1 Electromagnetic Induction (Eddy Current Testing)

In 1831 Faraday and Henry found that a moving magnetic field induces a voltage in a conductor. Such a method of producing current in a conductor by putting it in a varying magnetic field is termed as electromagnetic induction. In this process the current is induced in the conductor by the magnetic field [22].

Electromagnetic induction is the physical basis for all eddy current NDT techniques. The eddy current technique can be used for detection of zinc loss from the steel strands inside ACSR [51]. Detectors based on this principle can identify any flaws in a conductor well before other non-destructive tests can do. The feasibility studies on various detection methods by Komoda et al. [33] also prove that electromagnetic induction method is highly sensitive with excellent practicality.

3.1.1 Principle of Operation:

As soon as an alternating current flows in a coil near a conductor, the magnetic field of the coil induces eddy currents in the conductor. These eddy currents control the loading on the coil and consequently the impedance on it. If there is a flaw on the conductor's surface beneath the coil, it will decrease the flow of eddy currents, which reduces the loading on the coil and increases the impedance on it. This is the basic concept for eddy current inspection [22].

Consider a pair of probe coils forming the sensing head as shown in figure 3, with one of the coils acting as field winding while the other as pick-up coil. The sensing head is designed to traverse along the wire.

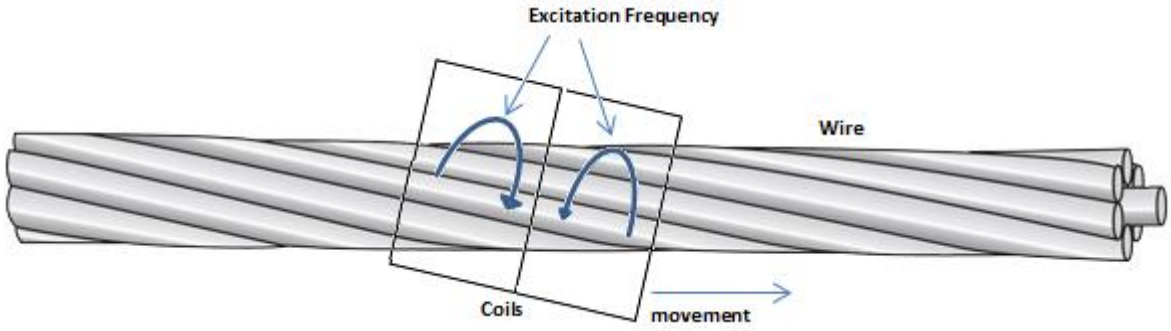

Figure 3: Principle of operation of eddy current testing method [33]

High frequency currents are passed through field windings and generate a magnetic field *H* that enter the conductor and induce eddy currents around each of the strands in the wire. These eddy currents produce alternating flux whose magnitude and phase are sensitive to any corrosion of the strands in the wire [51].

When the coils are traversed along a normal segment of the wire, the eddy currents in the wire induce some electromotive force in the coils with some particular impedance. On the contrary, when the coils are traversed over a corroded segment, the conductor induces a changed electromotive force on the coils, and the coils exhibit a change in the impedance. Thus, an uneven voltage is spotted on the pick-up coil. The detected voltage then undergoes numerous signal processing phases like amplification and phase detection to be further evaluated [33, 51]. This is the basic principle of eddy current testing.

There are a number of factors that can affect the response of eddy currents; these include the excitation frequency, material conductivity, permeability, geometry, flaws, and the position between the flaw and the coils [33]. Among these factors, the frequency and the geometry of the coil are important to effectively distinguish between corroded and normal conductors [33].

Sutton et al. [51] take this concept to further investigation and identify two component voltages namely "in-phase" and "quadrature" gained as output in this process. The in-phase voltage is only associated with aluminium strands while the steel strands are responsible for both in-phase and quadrature voltages.

The eddy currents induced around the strand constrain the flow of magnetic flux into the centre of the strand, and particularly at high frequencies this flux would be totally excluded from the whole strand cross-section [51].

The magnetic flux density is given by:

$$B = \mu_0 H = \mu_0 H_0 \sin(\omega t)$$

Let R be the radius of both field winding and the pick-up coil, and r be the radius of the strand.

The voltage induced in the coil is given by [51]:

$$V = -\frac{d\Phi}{dt}$$

Or

$$V = -\frac{dB}{dt} A = -\mu_0 H_0 (\pi R^2 - \pi r^2) \frac{d}{dt}(\sin \omega t)$$

$$V = -\mu_0 H_0 \omega \cos \omega t (\pi R^2 - \pi r^2) \quad ---------- (5)$$

In equation (5), part of the induced voltage, $-\mu_0 H_0 \omega \cos \omega t(\pi R^2)$, is not what we are looking for because it is associated with R, radius of the coils, and can be removed by introducing an identical "compensation" voltage, V_C, in the opposite direction [51].

Hence, the resultant voltage is:

$$V_m = V - V_C$$

$$V_m = -\mu_0 H_0 \omega \cos \omega t (\pi r^2) \quad ---------- (6)$$

This voltage is proportional to the area of the strand, i.e. $V_m \propto \pi r^2$

Equation (6) is applicable at very high frequencies only. If a detector is designed to operate at lower or intermediate frequencies then the penetration of flux into the strands needs to be considered. The penetration distance (skin depth) is given by [51]:

$$\delta = \sqrt{\frac{\rho}{\mu \pi f}} = \sqrt{\frac{2\rho}{\mu_o \mu_r \omega}} \quad ---------- (7)$$

Where, ρ is the electrical resistivity and μ_r is the relative magnetic permeability of the strand. μ_r

It can also be shown that for δ << r, the flux penetrating into the strand is given by

$$\phi_p = \pi r \mu_0 \mu_r \delta H_0 (\sin \omega t + \cos \omega t)$$

This flux possesses two equal components, one in phase with the applied field, $H_o \sin \omega t$, the other in phase quadrature. This flux induces a voltage, $\frac{d\phi_p}{dt}$, in the pick-up coil besides that due to flux exclusion, given in equation (6). The total voltage is [51]:

$$\frac{d\phi_p}{dt} = \pi r \mu_o \mu_r \delta H_o (w \cos \omega t - w \sin \omega t)$$

$$V p = w \pi r \mu_o \mu_r \delta H_o (\sin \omega t - \cos \omega t)$$

$$V_m = -\mu_o w H_o \pi r^2 [(1 - \frac{\delta \mu_r}{r}) \cos \omega t + (\frac{\delta \mu_r}{r}) \sin \omega t)]$$

Which reduces to equation (6) at high frequency as $\delta \longrightarrow 0$.

The feasibility study on different detection methods by Komoda et al. [33] suggests that the eddy current induction method is highly feasible for flaw detection, and finds that the method offers high sensitivity with outstanding practicality. Their findings are summarized in table 1 below.

Table 1: Comparison of various types of NDT techniques [33]

Technique	Sensitivity	Ease of use	Applicability	Feasibility
Electromagnetic Induction	o	o	o	o
Magnetic Flaw detection	o	×	×	×
Ultrasonic Method	^	×	×	×
Longitudinal Vibration	×	^	^	×
Bending Stiffness	×	o	^	×
Shooting Camera (visual)	^	^	^	^
Legend	Excellent: o	Fair: ^	Poor: ×	

3.2 Detectors Based on Eddy Current Technology Available in Market

Using eddy current technology for detection of corrosion on ACSR conductors, a number of detectors have been developed and commercialized. Some of the most popular ones around the world are introduced below.

3.2.1 Cormon OHLCD Technology

Overhead Line Corrosion Detector (OHLCD) is industrialized by Teledyne Cormon in cooperation with CEGB research organization and is widely used by companies in the UK, France and Sweden [6]. The detector encloses a winding and a pick-up coil and holds around the conductor. It can operate on any size ACSR dead line and also on live lines of up to 275kV. The manufacturer also claims that it can detect significant loss of aluminium cross section of up to 5% [6].

3.2.2 Fujikura's Detector

Fujikura's technology of internal corrosion analysis uses the eddy current inspection method and facilitates persistent and quantitative measurement of the internal corrosion. This technology was developed by Fujikura in cooperation with Tokyo Electric Power Company [15]. In order for the implementation of inspection work, two methods; manpower inspection and auto inspection are offered. So far, the detector has been embraced by ten major power companies in Japan like Hokkaido Electric Power Company and Kyushu Electric Power Company [15].

3.2.3 Detection Services offered by ATTAR in Australia

Advanced Technology Testing and Research, (ATTAR) [1], offers a NDT service for overhead line corrosion. It has more than 15 years of experience inspecting the condition of cables in the power industry. The device is positioned on live wires by a group of linesman and then operated remotely. It can be operated on lines with voltages over 500kV [1].

Chapter 4

- Transmission Line
- Transmission Line Parameters
- Transmission Line Modelling

Chapter 4: Transmission Line

4.1 Transmission Line

A transmission line is a medium which provides a route for transmitting energy from one place to another, such as electromagnetic waves or electrical energy. It usually comprises two or more parallel conductors used to establish a connection between generating units and distribution system which ultimately supplies the load [36]. Examples include electric power lines, wiring, coaxial cable, etc. Problems related to transmission lines are basically tackled by electromagnetic field theory and electric circuit theory. In this project the circuit theory is preferred to model the transmission line because it is easier to deal with mathematically.

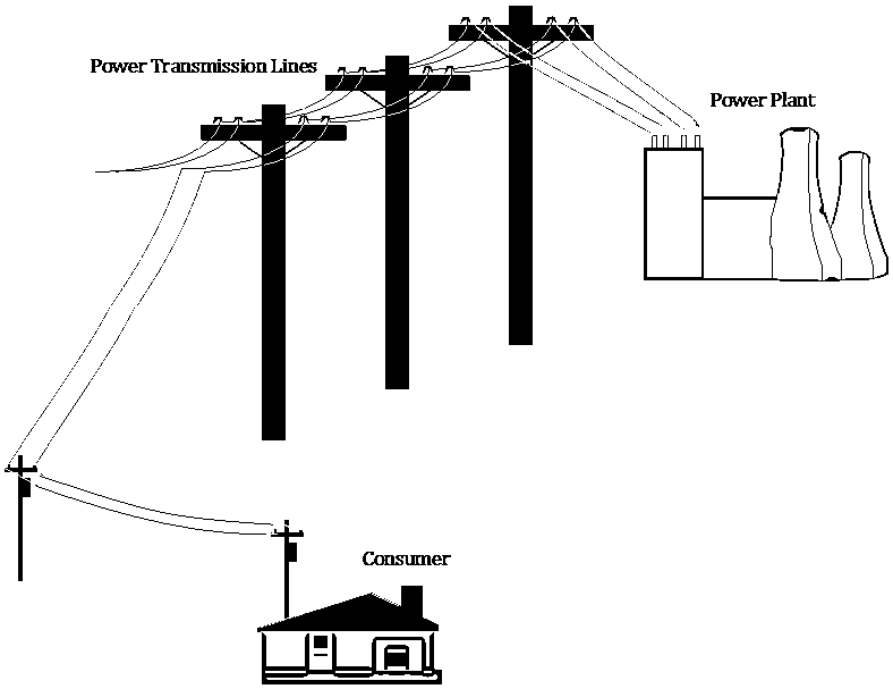

Figure 4: Power transmission lines

4.2 Transmission Line Parameters

Transmission Lines are usually described in terms of their line parameters including:

a. Series resistance per unit length *R;*

b. Series inductance per unit length *L;*

c. Shunt capacitance per unit length *C;*

d. Shunt conductance per unit length *G;*

4.2.1 Series Resistance

The *DC* resistance of a solid round conductor is given by [49]:

$$R_{DC} = \frac{\rho l}{A}$$

Where,

ρ = conductor resistivity (Ω-m);

l = conductor length (m);

A= conductor cross-sectional area (m^2);

In case of alternating current AC, the current distribution is not uniform over the cross-sectional area and the current density is higher at the surface of the conductor. As a result, the AC resistance is slightly higher than the DC resistance. This is known as the Skin Effect [49]. The conductor resistance is also dependent on temperature and spiralling. Due to these effects, the resistance of a conductor is best obtained from manufacturer's data.

4.2.2 Series Inductance

The inductance *L* is due to the effects of magnetic and electric fields around the conductor. Cable manufacturers usually provide the inductive reactance of the

conductor and hence, the inductance *L* can be calculated using the following formula [17]:

$$X_L = 2\pi f L \quad ----------(8)$$

In case of a three-phase transmission line the inductance per phase per kilometre length is given by [49]:

$$\mathrm{L} = 0.2 \ln \frac{D_{\mathrm{eq}}}{D_{\mathrm{s}}} \ (\frac{\mathrm{mH}}{\mathrm{km}}) \quad ----------(9)$$

Where, D_{eq}, the cube root of the product of three-phase spacing, is the geometric mean distance between phases in figure 5.

$$D_{eq} = \sqrt[3]{D_{\mathrm{ab}} * D_{\mathrm{bc}} * D_{\mathrm{ac}}}$$

Also, D_s is the geometric mean radius, GMR.

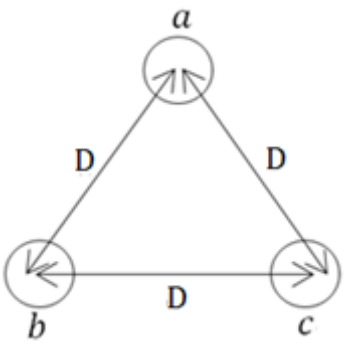

Figure 5: Three phase line

In case of using more than one conductor per phase, a practice called bundling, the series reactance and hence the inductance of the line is reduced due to the increase in GMR of the bundle. This improves the line performance and increases the power capability of the line [49]. Figure 6 shows a three-phase line with two conductor bundles, chosen randomly to investigate transmission line parameters in this project.

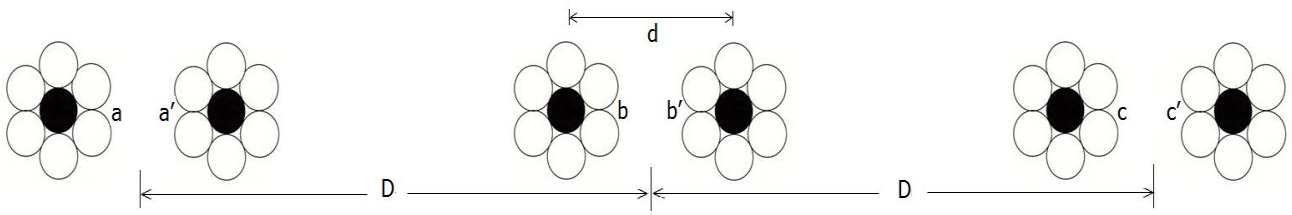

Figure 6: Three-phase, two-conductor bundled line

To calculate the inductance, "D_s" in equation 9 above is replaced by the GMR of the bundle, D_{SL} [49]:

$$\mathrm{L} = 0.2 \ln \frac{D_{eq}}{D_{SL}} \quad (mH/km)$$

Since the bundle constitutes a composite stranded conductor, i.e. ACSR conductor, first GMR of each stranded conductor (i.e. D_s) is worked out and then the bundle's GMR is calculated using equations (10) and (11) below.

For (6 by 1 aluminium to steel) ACSR conductor, GMR is approximated by [4]

$$D_S = 0.768\ \mathrm{r} \quad ----------(10)$$

Where, r is radius of each conductor.

And, for the bundle given above [17]:

$$D_{SL} = \sqrt{D_S * \mathbf{d}} \quad ----------(11)$$

Where **d** is the spacing between the sub-conductors in each phase.

4.2.3 Shunt Capacitance

Transmission line conductors show capacitance with respect to each other because of the potential difference between them. This capacitance depends on the conductor size, spacing, and height above the ground [49]. In case of a three-phase transmission line, the capacitance per phase per kilometre length is [17]:

$$C = \frac{2\pi \mathcal{E}o}{ln(\frac{D_{eq}}{r})} \quad (F/m) \quad ----------(12)$$

Where,

$$\mathcal{E}o = 8.854 \times 10^{-12} \quad (\frac{F}{m})\ ;$$

$$D_{eq} = \sqrt[3]{D_{\mathrm{ab}} * D_{\mathrm{bc}} * D_{\mathrm{ac}}}\ ;$$

$$r = \ radius\ of\ the\ conductor\ ;$$

In order to find the capacitance per phase for a three-phase transposed line with two-conductor bundle, the same steps are followed as the procedure for derivation of the inductance above [17].

$$C = \frac{2\pi\mathcal{E}o}{ln(\frac{D_{eq}}{D_{sc}})} \quad \left(\frac{F}{m}\right) --------------------------(13)$$

$$D_{SC} = \sqrt{\mathrm{r} * \mathbf{d}}$$

Where **d** is the spacing between the sub-conductors in each phase and r is the radius of each conductor.

4.2.4 Shunt Conductance

The shunt conductance accounts for leakage currents flowing across insulators and air. As leakage currents are considerably smaller compared to the current flowing through the transmission line, they may be neglected and hence, shunt conductance is usually not considered for transmission line modelling [49].

4.3 Transmission Line Modelling

Transmission lines may be represented by an equivalent circuit with suitable parameters on a per phase basis. The terminal voltages are shown from one line to neutral while the current is given for one phase. Therefore, a three-phase system is summarized by a comparable single-phase system.

For the purpose of wave propagation analysis in transmission lines two methods can be followed; the first is solving Maxwell's equations [36] with boundary conditions according to the system's physical nature, and the second is labelling the line by distributed parameter equivalent circuit and investigating the propagation of wave in terms of current and voltage [36].

In this project, long line theory is described and expressions relating to voltage and current for the distributed line model are developed.

4.3.1 Distributed Parameter Line Model (Long Line Model)

For long length lines (250 km and longer), in order to obtain more accurate solutions, the effect of the distributed parameters must be taken into account, i.e. the circuit parameters namely resistance, capacitance, and inductance are assumed to be distributed continuously along the length of the line, contrary to the lumped parameter model which assumes these values to be lumped together and connected by perfectly conducting wires.

A distributed equivalent circuit is shown below in figure 7. The length of the transmission line is denoted by *"l"*.

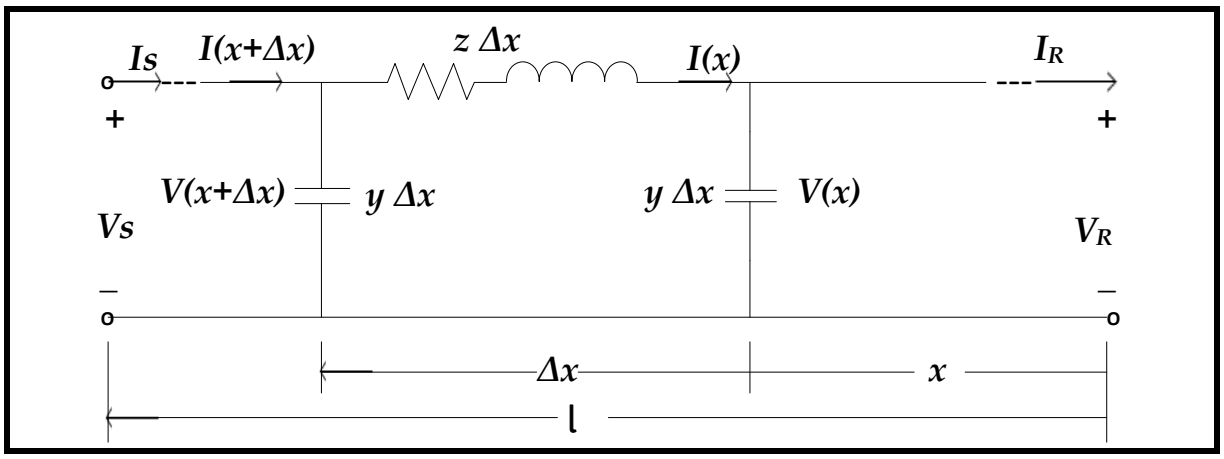

Figure 7: Distributed parameter equivalent circuit [49]

The circuit possesses a uniformly distributed series resistance *R*, series inductance *L*, shunt conductance G, and shunt capacitance *C*. The series impedance per unit length is denoted by z and the shunt admittance per phase by y.

Here,

$$z = R + jwL$$

$$y = G + jwC$$

Consider a small section Δx of the line at a distance *x* from the receiving end of the line in figure 7 above. The phasor voltage at the end of this segment is

$$V(x + \Delta x) = V(x) + z\,\Delta x\, I(x)$$

And the phasor current is

$$I(x + \Delta x) = I(x) + y\,\Delta x\, V(x + \Delta x)$$

Rearranging and solving these two equations gives us the second order differential equation

$$\frac{d^2V(x)}{dx^2} - \gamma^2 V(x) = 0$$

Note: Please refer to appendix D for derivation of all equations given in this section.

Where γ, known as the propagation constant, is a complex expression given by

$$\gamma = \alpha + j\beta = \sqrt{zy} = \sqrt{(R + jwL)(G + jwC)} \quad ----------(14)$$

The real part α is called the attenuation constant and the imaginary part β is known as the phase constant.

The characteristic impedance, Zc, defines the relationship between voltage and current in the line. It is given by [49]:

$$Zc = \sqrt{\frac{R + jwL}{G + jwC}}$$

The sending end and the receiving end of the line can be related by

$$V(s) = \cosh \gamma l \, V_R + Zc \sinh \gamma l \, I_R \quad ----------(15)$$

$$I(s) = \frac{1}{Zc} \sinh \gamma l \, V_R + \cosh \gamma l \, I_R \quad ----------(16)$$

Expressing this in ABCD constants

$$\begin{bmatrix} Vs \\ Is \end{bmatrix} = \begin{bmatrix} A & B \\ C & D \end{bmatrix} \begin{bmatrix} V_R \\ I_R \end{bmatrix}$$

Where,

$$\mathbf{A} = \boldsymbol{cosh}\ \boldsymbol{\gamma l} \qquad \mathbf{B} = \mathbf{Zc}\ \boldsymbol{sinh}\ \boldsymbol{\gamma l}$$

$$\boldsymbol{C} = \frac{\mathbf{1}}{\mathbf{Zc}} \boldsymbol{sinh}\ \boldsymbol{\gamma l} \qquad \boldsymbol{D} = \mathbf{A} = \boldsymbol{cosh}\ \boldsymbol{\gamma l}$$

We can replace the ABCD constants in the equivalent π −model shown in figure 8.

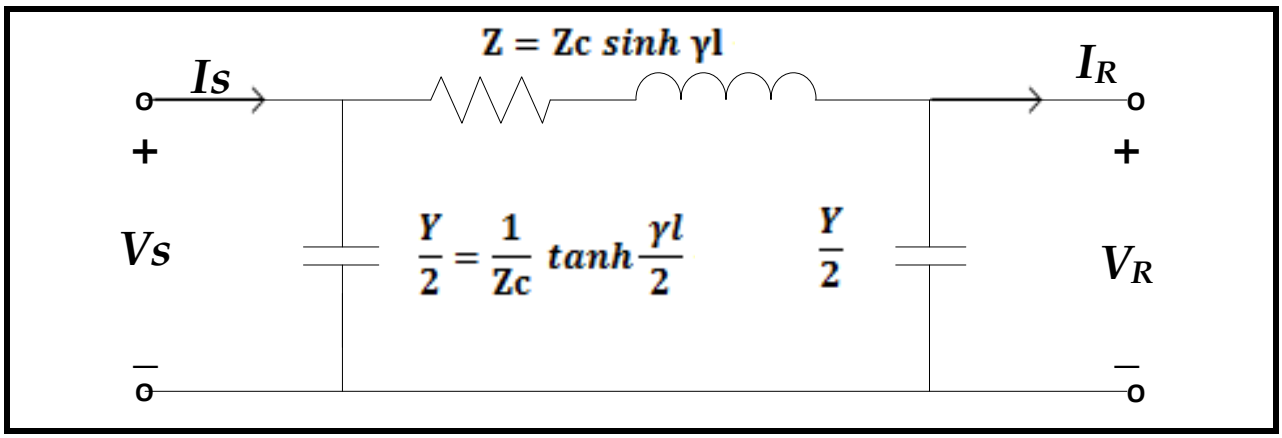

Figure 8: Equivalent π-model [49]

The following equations represent the parameters of the equivalent π −model. Please see appendix D for detailed calculation of all equations in this section.

$$\mathbf{Z = Zc}\ \boldsymbol{sinh}\ \boldsymbol{\gamma l}$$

$$\frac{\mathbf{Y}}{\mathbf{2}} = \frac{\mathbf{1}}{\mathbf{Zc}}\ \mathbf{tanh}\frac{\boldsymbol{\gamma l}}{\mathbf{2}}$$

Chapter 5

- Time Domain Reflectometry
- Reflection from Typical Load Terminations
- Transients in Transmission Line TDR
- Some Important Factors in TDR Analysis

Chapter 5: Time Domain Reflectometry

5.1 Time Domain Reflectometry

A very common method for evaluation of transmission lines has been the application of sine wave to a system and measuring the standing waves due to irregularities on the line. The measurements are then used to calculate the standing wave ratio, SWR, which can be helpful for the investigation of the transmission system [28]. However, the SWR technique fails to operate when there are several discontinuities. Moreover, if the system is composed of a connector, a short line with a load, the SWR identifies the whole quality of the system; it cannot detect which component in the system is responsible for the reflection [28]. Thus, it requires extensive measurements at various frequencies before one can reach a satisfactory conclusion. For this reason it is assumed to be very time consuming and tedious.

In comparison to other methods, time domain reflectometry (TDR) offers instinctive and simple analysis of the device under test. It provides more significant information about the characteristics of a transmission system than any other techniques [25]. This type of reflectometer has been practiced by engineers since 1930s for evaluating characteristics of transmission lines and spotting faults [52]. TDR is an electrical testing technique generally used to determine the location and condition of a device under test. It operates on the same principle as radar with the exception

that the medium is a wire rather than air [52]. As the basic principles of TDR are effortlessly grabbed, one with low level of experience even, can quickly grasp this technique.

5.1.1 Principle of Operation

Time domain reflectometry is another NDT method to detect and locate faults in transmission lines. This method involves sending an electrical pulse (usually a short step) along a transmission line and observing the returning pulse energy using an oscilloscope [47]. The principle of TDR is shown in figure 9 below.

When the load impedance Z_L matches the characteristic impedance of the line Z_C no reflection occurs and the oscilloscope records the incident voltage step only, as seen in figure 10(a). On the other hand, when the signal travelling in the line encounters any impedance change, part of the incident wave is reflected back. This is in fact the energy that is not passed on to the load. The reflected voltage wave then appears on oscilloscope in addition to the incident wave [47] as shown in figure 10(b).

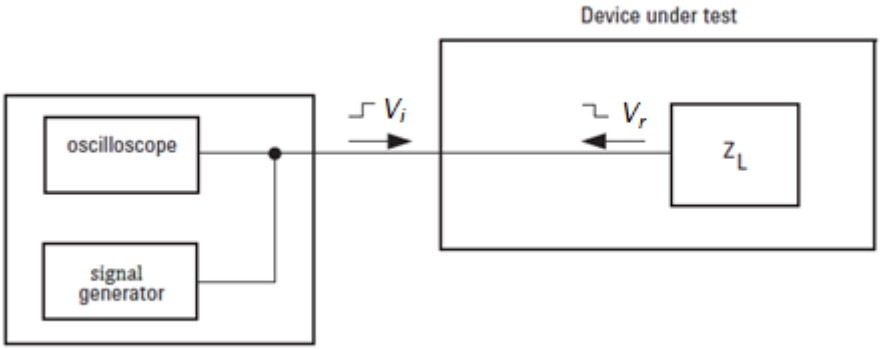

Figure 9: Block diagram of a time domain reflectometer [25]

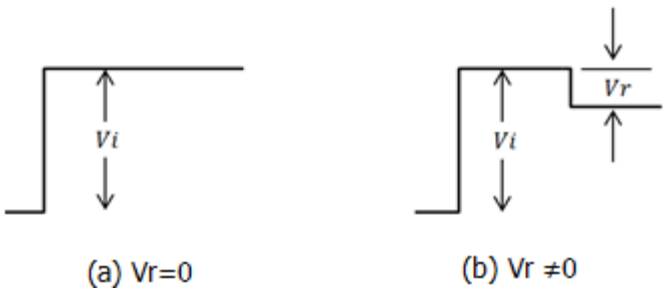

Figure 10: Oscilloscope displays [28]

The magnitude of the reflected signal can be calculated using reflection coefficient Γ, which is also, in frequency domain, the ratio between reflected voltage wave V_r and the incident voltage wave V_i[26].

$$\Gamma = \frac{V_r}{V_i} = \frac{Z_L - Z_c}{Z_L + Z_c} \quad ----------(17)$$

In addition, part of the incident wave may be transmitted through the load. The relation between the transmission coefficient and reflection coefficient are related by the expression [25]:

$$\mathrm{T} = 1 + \Gamma = 1 + \frac{Z_L - Z_c}{Z_L + Z_c}$$

$$\mathrm{T} = \frac{2Z_L}{Z_L + Z_c}$$

From this we can get the amplitude of the transmitted pulse through the point of impedance mismatch as:

$$V_t = TV_i$$

Figure 11 displays the reflection coefficient Γ and the transmission coefficient T in TDR measurement.

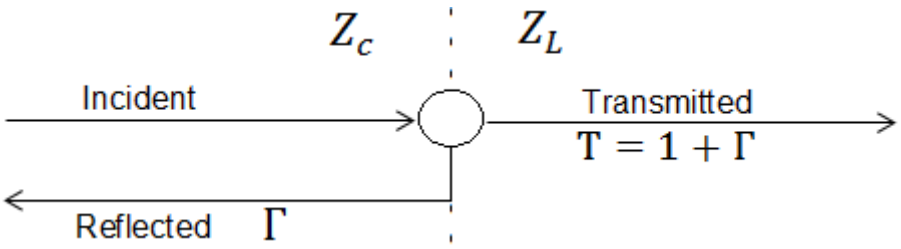

Figure 11: Transmission and reflection coefficient

5.2 Reflection from Typical Load Terminations

The shape of the reflected wave is an important parameter as it unveils the nature and magnitude of the impedance mismatch or the load [28]. Displays from the

oscilloscope can be easily interpreted using equation (17). Some particular load terminations and the associated reflected waveforms are discussed here.

5.2.1 Open Circuit Termination

A transmission system terminated with an open circuit can be represented with a load of infinite impedance. In this case there is no current passing through the load, while the voltage is maximum.

Using equation 17 for $Z_L = \infty$

$$\Gamma = \frac{V_r}{V_i} = \frac{\infty - Z_c}{\infty + Z_c} = 1$$

yields to,

$$V_r = V_i$$

In case of open circuit termination the reflected voltage $(Vr = Vi)$ is added to the incident voltage. Figure 12(a) shows the open circuit termination and the waveform associated with it.

5.2.2 Short Circuit Termination

A transmission system terminated with a short circuit can be represented with a load of zero impedance. Using equation 17, for $Z_L = 0$

$$\Gamma = \frac{V_r}{V_i} = \frac{0 - Z_c}{0 + Z_c} = -1$$

yields to,

$$V_r = -V_i$$

In case of short circuit termination the reflected voltage ($V_r = -V_i$) is added to the incident voltage. Figure 12 (b) shows the short circuit termination and the waveform associated with it.

5.2.3 Matched Impedance Termination

A transmission system terminated with matched impedance is represented with $Z_L = Z_C$. Again using equation 17, for $Z_L = Z_C$

$$\Gamma = \frac{V_r}{V_i} = \frac{Z_C - Z_C}{Z_C + Z_C} = 0$$

yields to,

$$V_r = 0$$

In case of matched impedance termination the reflected voltage ($V_r = 0$) is added to the incident voltage. Figure 12c shows the short circuit termination and the waveform associated with it.

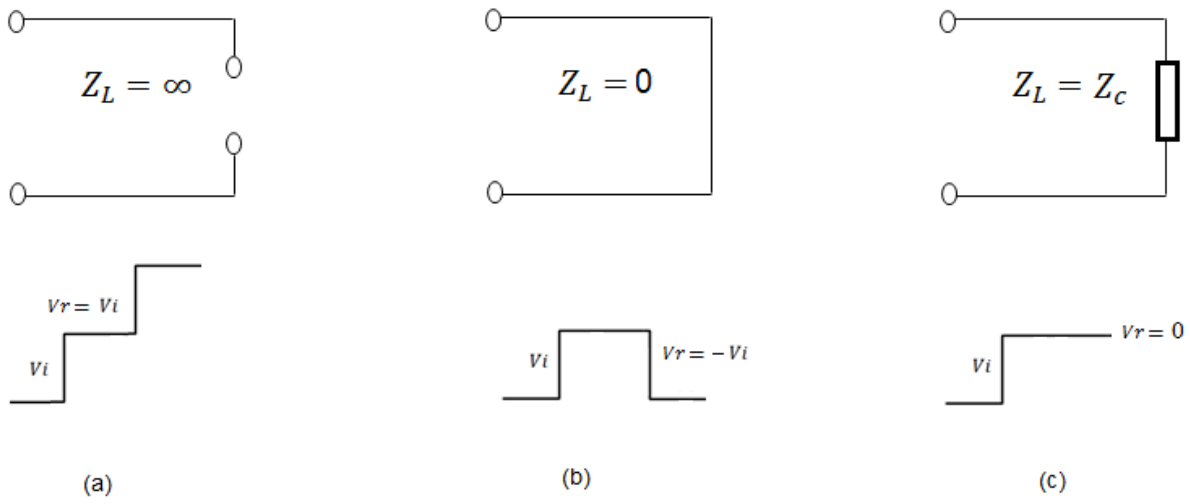

Figure 12: Typical load terminations and their respective waveforms

5.2.4 Complex Load Impedances

In the above sections various resistive load terminations and their associated waveforms were considered. It was observed that the mismatched impedances reflected a wave with the same shape as the incident wave, while the magnitude and polarity of V_r was found using the values of $\mathrm{Z_L and\ Z_C}$.

On the other hand, complex load impedances can also be measured by the TDR method [43] using the simple system shown in figure 9. The analysis involves evaluation of the reflected voltage at $t = 0$ and at $t = \infty$, where $t = 0$ shows the time when the reflected voltage arrives back at the oscilloscope. Figure 13 shows basic examples of complex load reflection. Considering the case of series R-L combination, at time $t = 0,$ the reflected wave is V_i. The reason is that the inductor does not take an abrupt variation in current, so first it looks like an open circuit [28]. After a short while the current in the inductor starts to build up exponentially dropping its impedance down to zero as shown in figure 13(a).

Similarly, in case of parallel R-C, at time $t = 0$, the reflected wave is $-V_r$. The reason is that the capacitor does not take an abrupt variation in voltage, so at first it looks like a short circuit ($\Gamma = -1$). After a short while the voltage starts to build up exponentially on the capacitor increasing its impedance to infinity at $t = \infty$ [28]. This is shown in figure 13 (b).

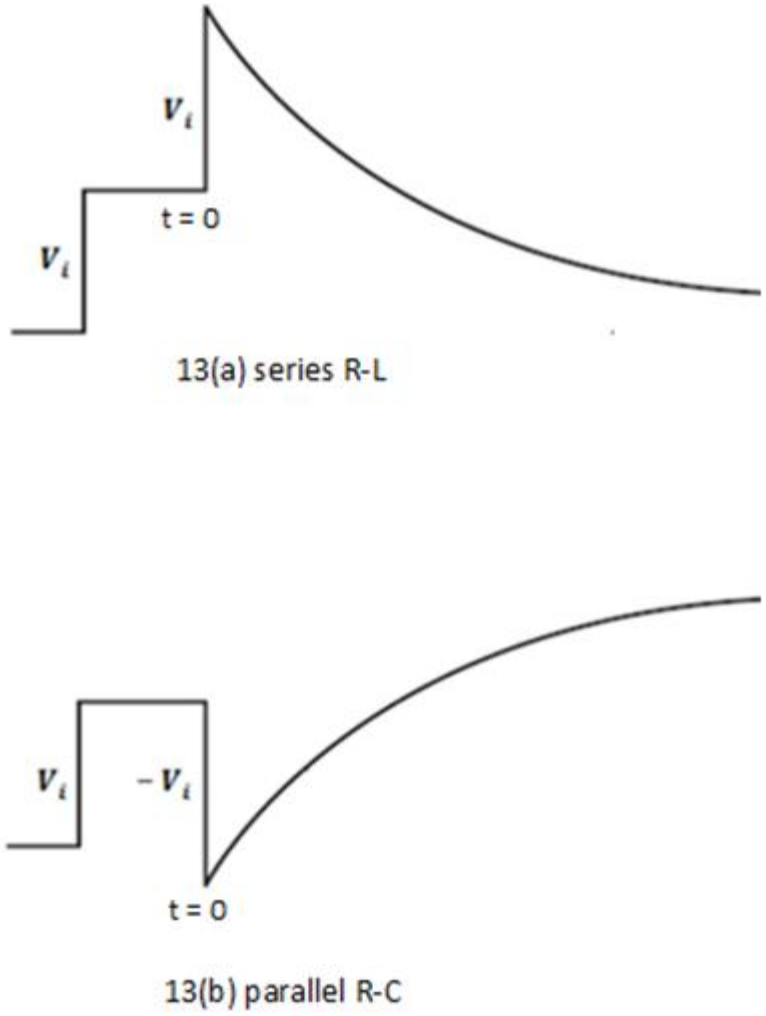

Figure 13: TDR display for complex loads [28]

5.3 Transients in Transmission Tine TDR

In practical applications when a pulsed signal is injected through a line, from Fourier analysis [21], we know that the pulse can be regarded as a superposition of waves of many frequencies. Therefore, a pulsed signal may be considered as simultaneous waves of different frequencies [21].

When the pulse is injected through the line, it takes some time for the voltage to reach a steady state value. This transitional period is called the transient. Usually, the transient behaviour is analysed in the frequency domain by Laplace transform [34], but for the sake of convenience, it can be treated in the time domain.

Consider a transmission line of length "l" and characteristic impedance Z_c as shown in figure 14 below.

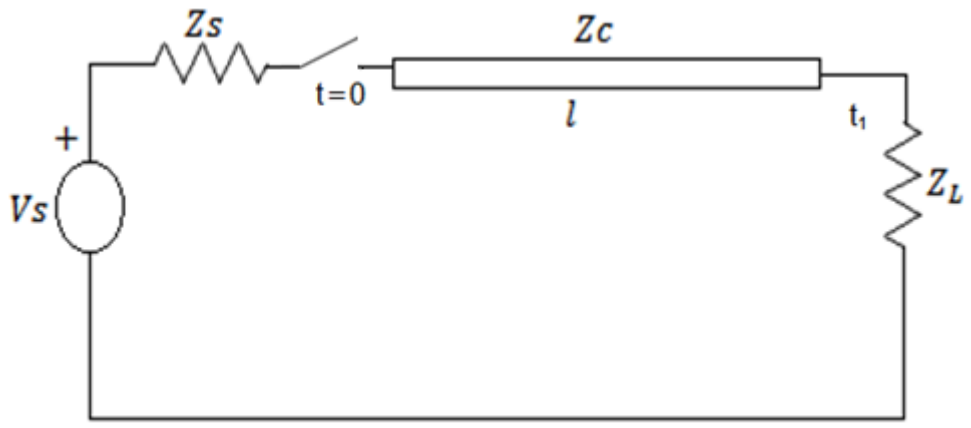

Figure 14: Transient on transmission line

Suppose that the line is driven by a pulse generator of voltage V_s with internal resistance Z_s and terminated with a resistive load Z_L. At the instant t = 0, the switch is closed. The starting current "sees" only Z_s and Z_c, so the initial voltage at t = 0+ is given by

$$V(t_0{}^+) = V_i = V_s(\frac{Z_C}{Z_C + Z_s})$$

After time t_1, the pulse reaches the load and some part of it is reflected back due to the mismatch. The voltage at the load is the sum of the incident and reflected voltages. Thus

$$V(t_1^+) = V_i + V_r = V_i + \Gamma_L V_i = (1 + \Gamma_L)V_i$$

Where, Γ_L is the reflection at the load given by:

$$\Gamma_L = \frac{Z_L - Z_c}{Z_L + Z_c}$$

The reflected wave V_r travels back towards the source in addition to the initial wave V_i already on the line. At time 2t the reflected wave reaches the source, so the voltage at the source just after time 2t is:

$$V(t_2^+) = V_i + \Gamma_L V_i + \Gamma_s \Gamma_L V_i = (1 + \Gamma_L + \Gamma_s \Gamma_L)V_i$$

Where, Γ_s is the reflection at the source given by:

$$\Gamma_s = \frac{Z_s - Z_c}{Z_s + Z_c}$$

Again the reflected wave from the source end propagates towards the load and the process continues until the energy is absorbed by the resistors Z_s and Z_L. The process of tracing the voltage back and forth gets complicated after a few reflections, therefore, it is more convenient to keep track of the reflections using a bounce diagram, otherwise known as a lattice diagram [20] shown in figure 15 below.

5.3.1 The Bounce Diagram

The bounce diagram shows a zigzag line indicating the position of the voltage with respect to the source end and its value after each reflection given by the letters a, b, c and so on. On the bounce diagram, the voltage at any time may be determined by adding these values.

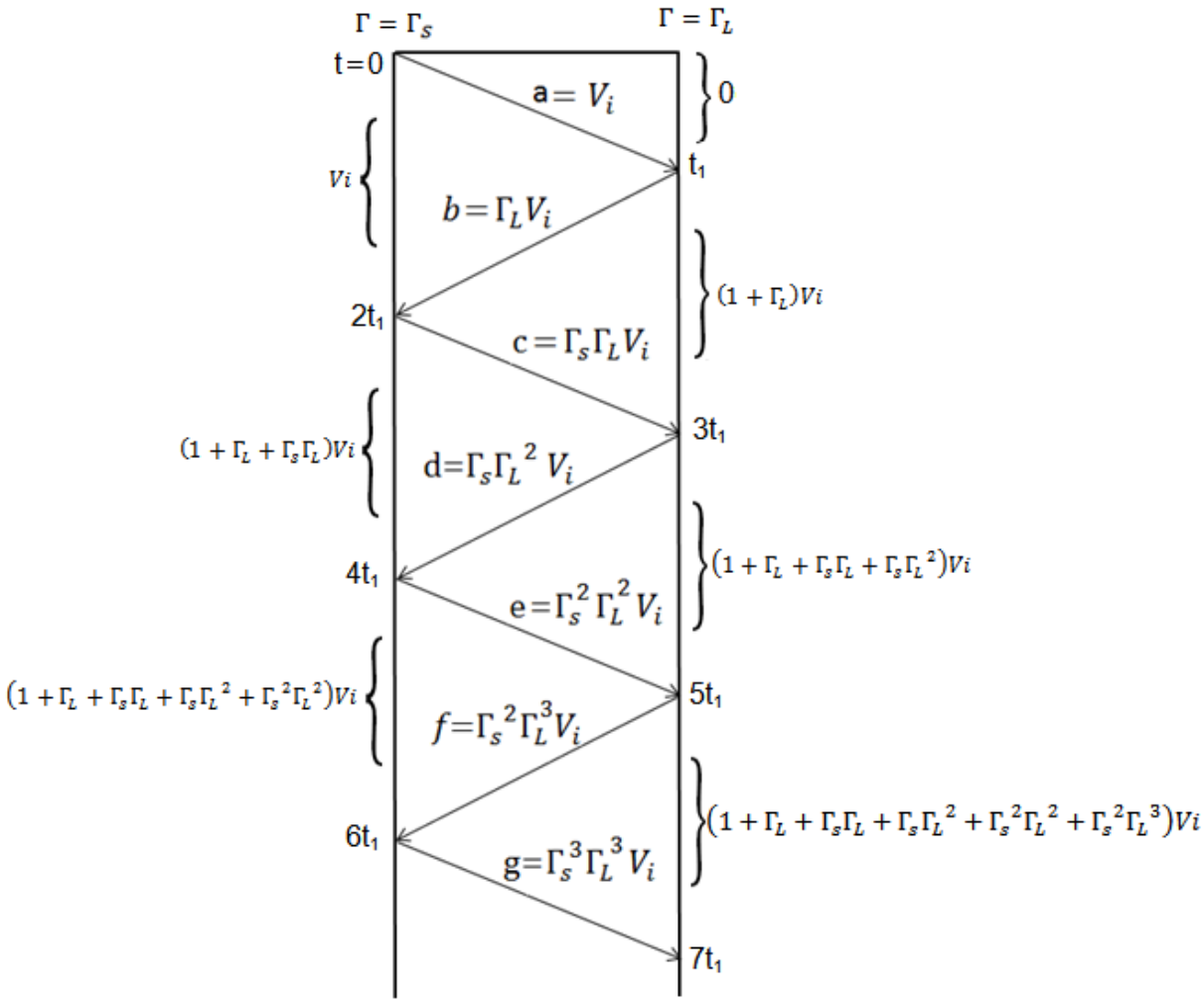

Figure 15: Voltage bounce diagram [20]

For the sake of clarification let us assume an example with the parameters $Z_s = 100\Omega$, $Z_c = 50\Omega$, $Z_L = 200\Omega$ and $V_s = 12V$. The initial voltage at the sending end is:

$$V_i = V_s\left(\frac{Z_C}{Z_C+Z_s}\right) = 4V$$

The voltages at each end and their corresponding voltage reflections are given in the figure 16.

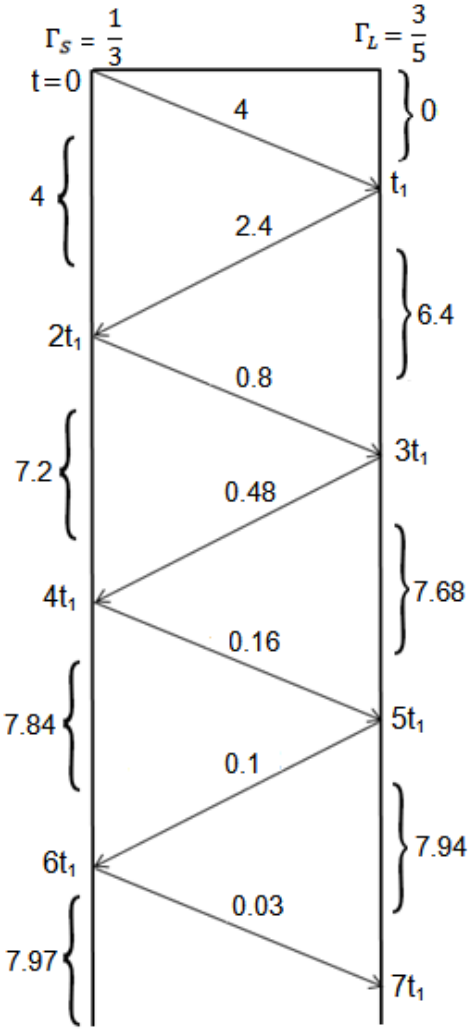

Figure 16: Voltage bounce diagram for the example under consideration

5.4 Some Important Factors in TDR Analysis

5.4.1 Propagation Velocity

Propagation velocity is a measure of a conductor's characteristic that specifies the speed at which a signal moves through it. Different conductors possess different velocity of propagation. Usually, the procedure is to send an electromagnetic signal through one end of a known length of the conductor and measure the time it takes to reach the other end to calculate propagation velocity. A more accurate way to work out the velocity of propagation is to repeat this process from both ends of the conductor.

We can also find the propagation velocity of a conductor without conducting an experiment on it. The velocity at which the signal moves down the line is measured in terms of phase constant β and the frequency of the signal. Mathematically given by [49]:

$$v_p = \frac{\omega}{\beta} = \frac{2\pi f}{\beta} \quad ----------(18)$$

Where,

$$\beta = \omega\sqrt{LC}$$

Therefore,

$$v_p = \frac{\omega}{\omega\sqrt{LC}} = \frac{1}{\sqrt{LC}} \quad ----------(19)$$

5.4.2 Calculation of Location of Mismatch Impedance

The reflected signal is easily distinguished as it is different in time from the initial signal. This time "t" is useful to find the distance d of monitoring point to the mismatch.

$$d = v_p \frac{t}{2} \quad ----------(20)$$

Where, t is the transit time from measurement point to the mismatch and then back to the measurement point.

One can read t from the oscilloscope to determine d and locate the mismatch down the line.

5.4.3 Characteristic Impedance

The characteristic impedance Z_C defines the relationship between voltage and current in the line. It is given by [49]:

$$Zc = \sqrt{\frac{R + j\omega L}{G + j\omega C}}$$

In case of a lossless transmission line, the characteristic impedance of the line is approximated by:

$$Zc = \sqrt{\frac{L}{C}}$$

Chapter 6

- Calibration of TDR measuring System
- Modelling in SimpowerSystems Toolbox
- Modelling corrosion in the cable
- Confirmation of Appropriate Circuit Design

Chapter 6: Application of TDR in this Project

6.1 Calibration of TDR Measuring System

The main problem in this project is to detect and locate corrosion in ACSR cables of overhead transmission lines. In order to investigate this problem let us consider an overhead transmission line consisting of ACSR conductor with the geometry given in figure 6. For the sake of ease this figure is reproduced here in figure 17 with specified distances between the bundles and the conductors. The conductor chosen for this transmission line is "**Hare**" from General Cable data sheet which is a 6 by 1 aluminium to steel strand ratio as shown in appendix B.

The overall length "l" of this transmission line is assumed to be 250 km. Moreover, we assume that there exists corrosion at different lengths of this line which will be, later, simulated to support the theory of fault localization using TDR technique.

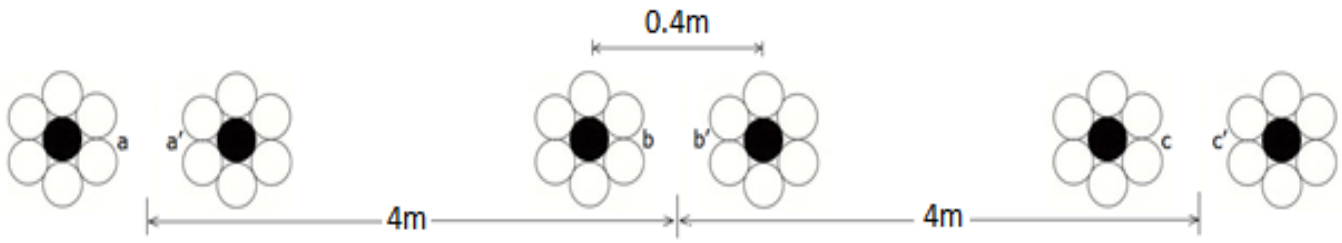

Figure 17: Three-phase bundled line used for TDR

The parameters for this transmission line are calculated using the equations described in section 4.2.

The resistance per unit length of this transmission line, as given in the General Cable data sheet is:

$R = 0.33\ \Omega/km$;

The inductance per unit length is (see appendix A for calculation)

$L = 0.94\ \mathrm{mH/km}$;

And the capacitance per unit length as calculated in appendix A is

$C = 12.2\ nF/km$;

The characteristic impedance of this line is

$Zc = 277\Omega\ \ (\text{see appendix A for calculation})$

Consider figure 18 where a pulse generator of internal resistance Zs is used to inject a step pulse though this line which terminates at a load of impedance Z_L. The pulse travels down the line with a velocity of propagation $v_p$calculated from equation 19 above.

$v_p\ = 2.95 \times 10^5 km/s$

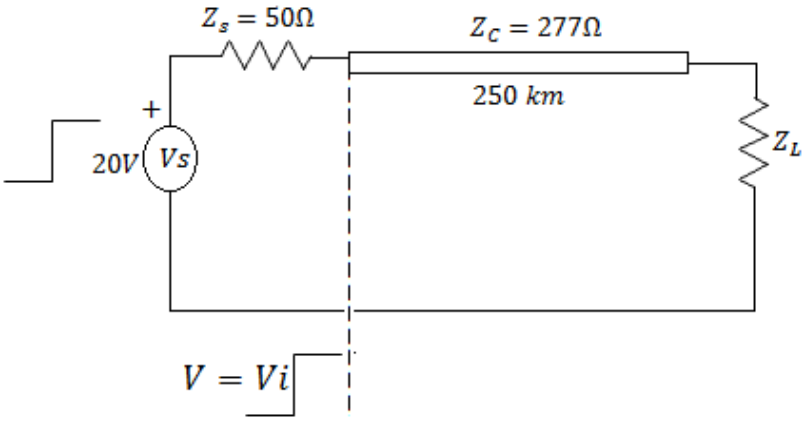

Figure 18: Pulse movement along the transmission line

The propagation time for this pulse is

$$t_p = \frac{l}{v} = \frac{250km}{2.95\frac{km}{s}} \times 10^{-5}$$

$t_p = 0.847\ ms$

In the next step we will implement this circuit in SimPowerSystems [38] which is a toolbox for modelling and simulating electrical power systems.

6.2 Modelling in SimPowerSystems Toolbox

There are many circuit simulators available like PSpice, CircuitLab etc. that can be used to conduct TDR analysis. However, in this project, SimPowerSystems [38] Toolbox in Simulink has been chosen.

SimPowerSystems [38] provides analysis tools for modelling and simulating electrical power systems. The models can be used to develop control systems and test system-level performance. They can also be parameterized using MATLAB variables and expressions, and design control systems for electrical power system in Simulink [38].

The basic block diagram for TDR analysis in SimPowerSystems is shown below in figure 19.

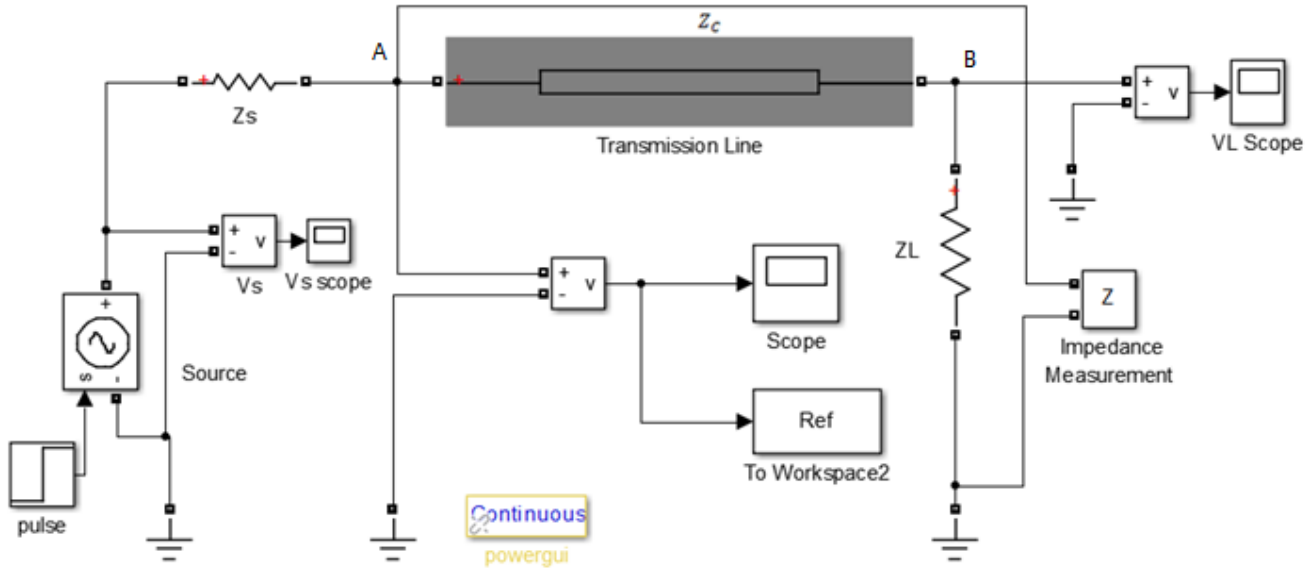

Figure 19: Block diagram for TDR analysis on transmission line

In this block diagram, the transmission line is represented by a distributed parameter line model. According to SimPowerSystems' user guide [38], this model relies on the principle of Bergeron's traveling wave which is used in the Electromagnetic Transient Program. According to this model, the ideal distributed line is characterized by two values: the characteristic impedance $Z_C = \sqrt{\mathrm{LC}}$ and the propagation velocity $v_p = \frac{1}{\sqrt{LC}}$, [38].

These equations give the same values which were calculated in previous section:

$$Z_C = 277\Omega$$

And

$$v_p = 2.95 \times 10^{-5} \frac{km}{s}$$

The values of the system parameters comprising ACSR conductor "Hare", from the circuit in figure 18 are entered here in the corresponding parameter block of the distributed parameter line. A pulse of 20V amplitude is provided through the source with impedance $Z_s = 50\Omega$, while the load Z_L is being varied for different simulation purposes. Initially the incident voltage $V_i = V_s\left(\frac{Z_c}{Z_c+Z_s}\right)$, enters the line at point A. After a propagation delay of $t_p = 0.847ms$, the signal arrives unchanged at the other end of the line at point B. Part of this signal $V_r = \Gamma V_i$, is reflected back from the load. This reflected signal, in addition to the incident one is then measured at point A on the scope shown in figure 19. It is also sent to Matlab's workspace for further investigation.

The step time for the injected pulse is 0.1ms while the total simulation time for the circuit is 10ms, keeping in mind the propagation time t_p, so that there is enough time for multiple to-and-fro motion of the wave.

6.3 Modelling Corrosion in the Cable

In case of corrosion in the cable, the electrical properties of the conductor change and hence the corrosion can be modelled as an electrical discontinuity. In SimPowerSystems it can be represented by a resistor whose impedance is different from the characteristic impedance of the transmission line. Therefore, when the circuit is run for TDR analysis, the impedance mismatch due to corrosion is detected and its distance from the point of observation is worked out. Moreover, it is assumed that there are no discontinuities present on the line other than the planted corrosion.

6.4 Confirmation of Appropriate Circuit Design

In the first stage of simulation, the circuit is run to check whether TDR operated correctly with this arrangement. For this purpose, the load is set to open circuit, short circuit and finally matched to Z_c, and the results are compared to the theory explained in section 5.2. This is depicted in Figure 20 (a), (b), (c).

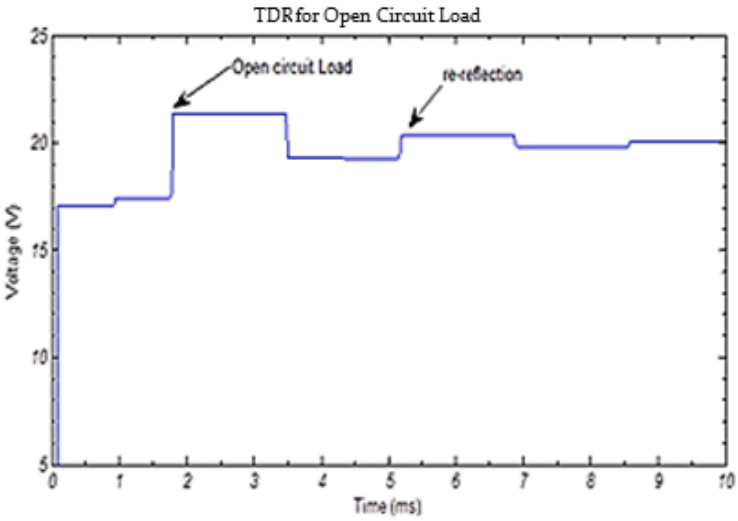

Figure 20(a) TDR result from open circuit load

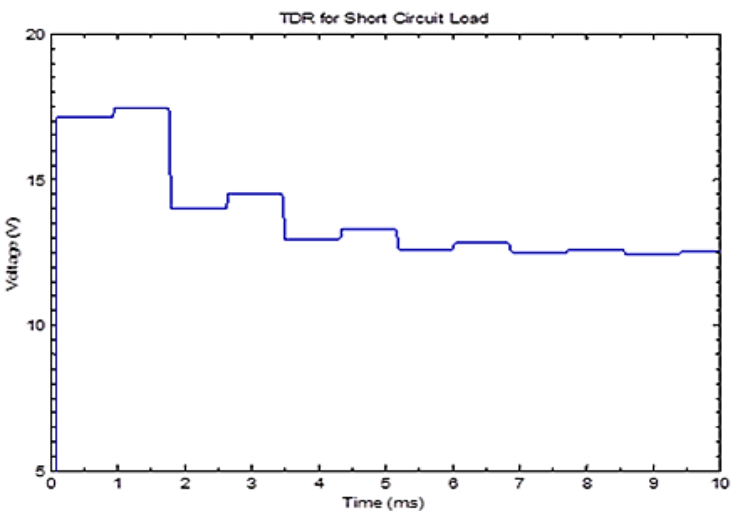

Figure 20(b): TDR result from short circuit load

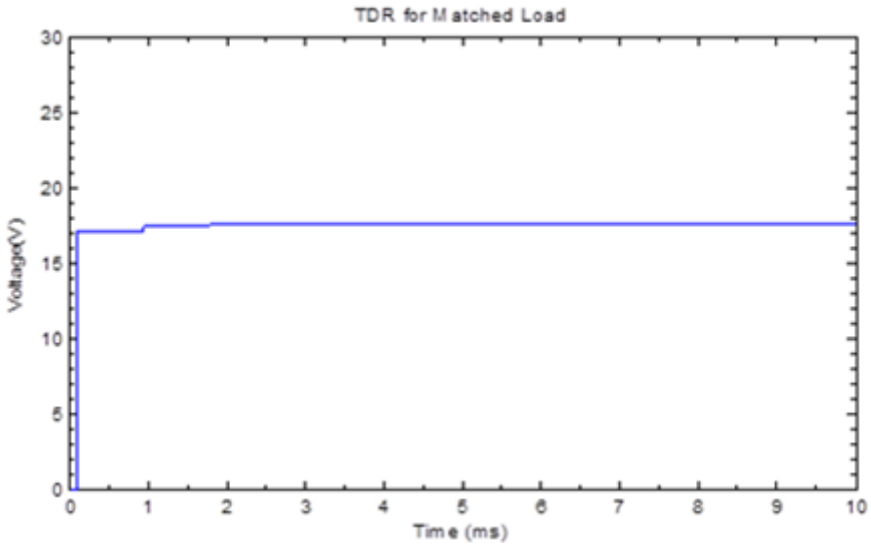

Figure 20(c) TDR result from matched load

It can be seen in figure 20(a) that the reflection from the open circuit load is positive and therefore added to the incident wave while the reflection from the short circuit load in figure 20(b) is negative and hence subtracted. In case of $Z_L = Z_c$, there is zero reflection in figure 20(c) and the incident wave remains as unchanged.

The above results when compared with theory, confirm the proper design of this circuit and hence it can be further used for detection and localization of corrosion in the cable.

Chapter 7

- Detection and Localization of corrosion
- Multiple corrosions:

Chapter 7: Simulation Results and Discussion

7.1 Detection and Localization of Corrosion

The length of the transmission line under consideration was chosen to be 250km. in order to detect corrosion at various distances, the line is further divided into segments of smaller length, all summed up together as seen in figure 21 below. In the next step, the impedance Z_m (usually 50 Ω unless otherwise stated) is planted at different known locations on the line and the circuit is simulated for TDR analysis. Moreover, the load impedance is kept equal to the characteristic impedance of the line so that any reflection from the load is avoided.

In practice, the transmission lines are joined by means of connectors which can cause anomalies to the pulse propagation. Additionally, there are a number of other components like suspension clamps, spacers, dampers, armor rods, etc. that may lead to discontinuity in the signal. However, in this project, it is assumed that there are no discontinuities present on the line. This process is shown in figure 21 below.

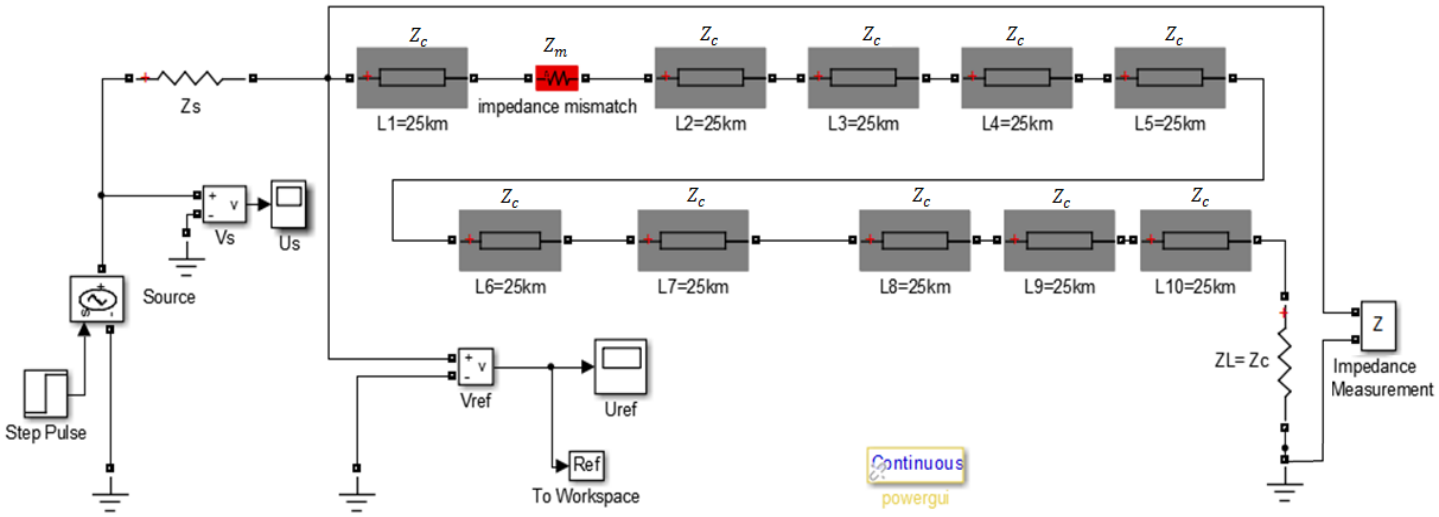

Figure 21: Corrosion planted at 25km on the line

At this stage in the circuit, a manipulated impedance mismatch representing corrosion in the cable is set at 25km from the source along the length of the line. The circuit was then simulated and the result is shown in figure 22 below.

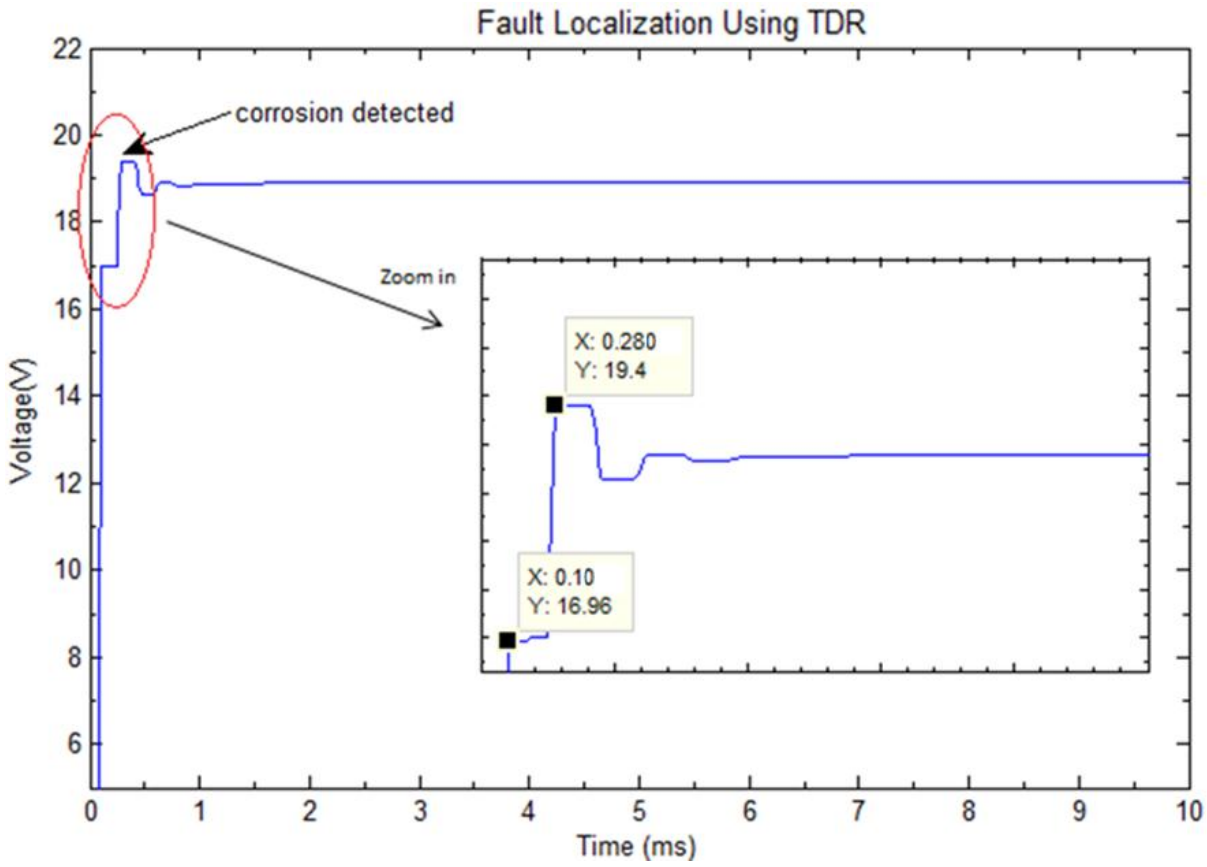

Figure 22: TDR Result for corrosion at 25 km

The graph in figure 22 shows that the incident voltage is about 17 V which tallies with the calculation, i.e.

$$V_i = V_s\left(\frac{Z_C}{Z_C + Z_s}\right) = 20(\frac{277}{277 + 50})$$

$$V_i = 17\ V$$

Moreover, it can be seen that a reflection is detected due to the impedance mismatch. This graph is zoomed in order to find the time of the occurrence of reflection more precisely.

The step time of the pulse is 100μs while the detected reflection appears at 280μs. The difference between the two shows the period that the wave has travelled to the fault point and back again to the measuring point where it was detected. In order to find the location of this fault, equation (20) is used.

$$d = (2.95 \times 10^5)\left(\frac{0.28-0.1}{2} \times 10^{-3}\right)$$

$$d = 26.55\ km$$

Hence, the corrosion in the cable of the transmission line is detected and localized to be at 26.55km while the actual fault location was 25km, an error of 6.2%.

This process of simulation was then continued for three more samples where the impedance mismatch due to corrosion was set at 100km, 150km and 200km. the corresponding TDR results and their interpretations are given below.

Figure 23 shows TDR fault localization due to corrosion at 100km from the measuring end of the line. As shown, the incident signal has the same initial amplitude of 17V at 100µs, and the reflection is detected at 800µs.

The measured corrosion is found to be located at 103.3km compared to the actual location of 100km, which is an error of 3.3%.

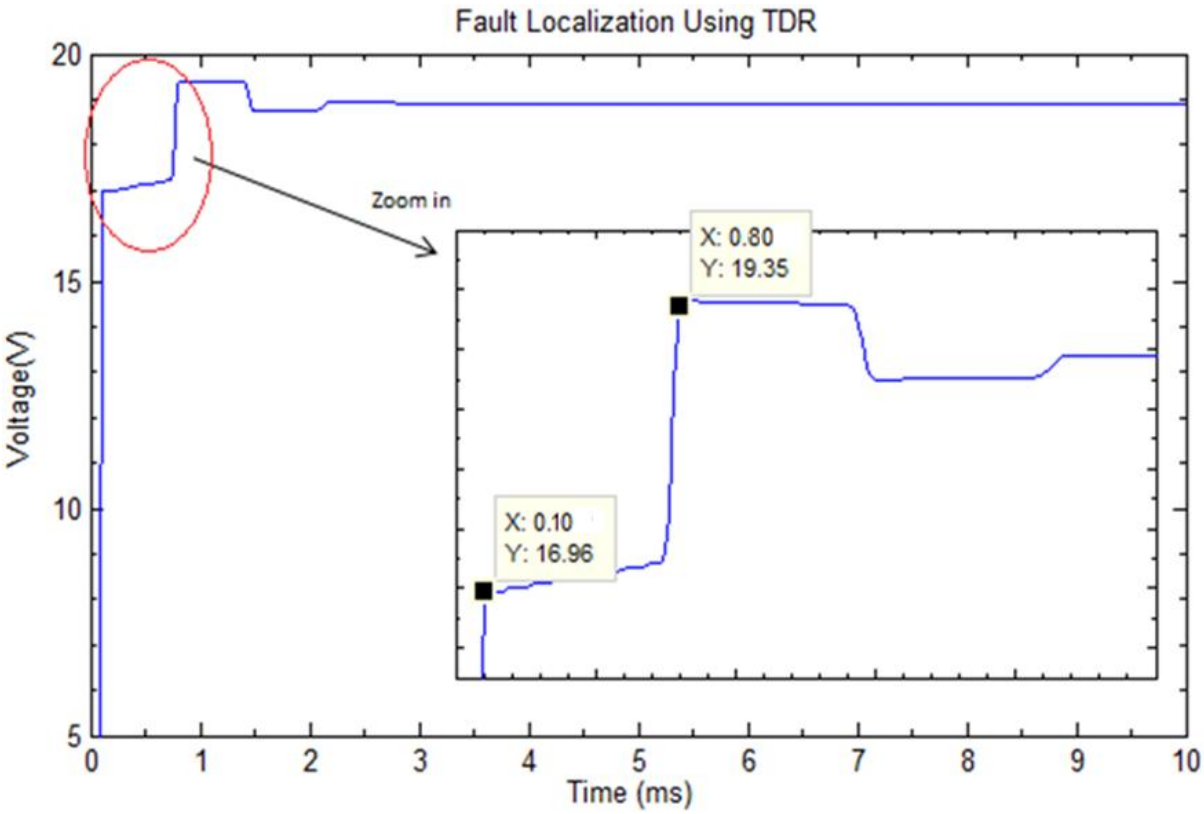

Figure 23: TDR Result for corrosion at 100 km

Figure 24 below shows the TDR outcome for corrosion at a distance of 150km. As shown, the incident signal has the same initial amplitude of 17V at 100μs, and the reflection is detected at 1.15ms.

The measured corrosion is found to be located at 154.9km compared to the actual location of 150km, an estimation error of 3.3%.

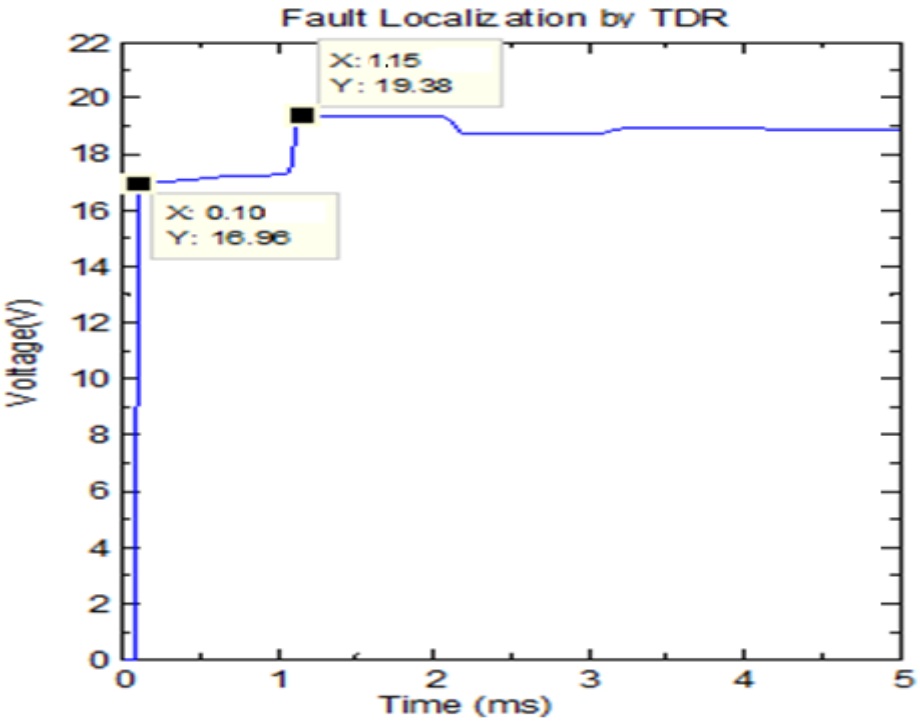

Figure 24: TDR Result for corrosion at 150 km

Figure 25 shows TDR fault localization due to corrosion at 200km from the measuring end of the line. As shown, the incident signal has the same initial amplitude of 17V at 100µs, and the reflection is detected at 1.49ms.

The corrosion in the cable is detected at 205km compared to the actual location of 200km, which is an estimation error of 2.5%.

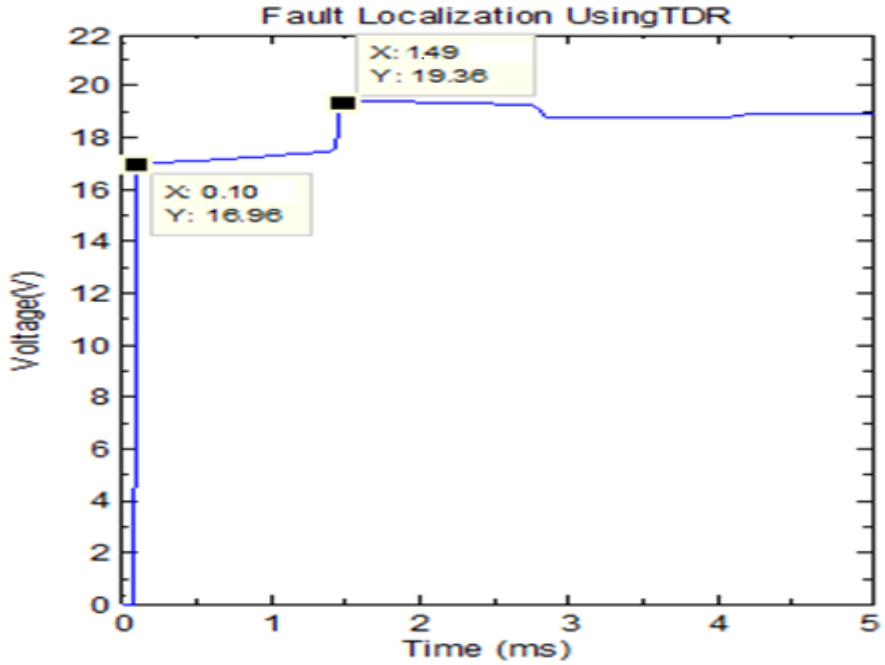

Figure 25: TDR Result for corrosion at 200 km

The results for all measured samples are combined and displayed in table 2.

Table 2: The overall TDR result for each single fault on the line

Actual Fault Location (km)	Step Time (s)	Fault Time (s)	Measured Fault Location (km)	Error (%)
25	1.00E-04	2.80E-04	26.6	6.2
100	1.00E-04	8.00E-04	103.3	3.3
150	1.00E-04	1.15E-03	154.9	3.3
200	1.00E-04	1.49E-03	205.0	2.5

7.2 Multiple Corrosions

As transmission lines run long distances through the environment, it is possible for corrosion to occur at multiple points on the conductor along the line. Therefore, the technology under consideration was tested for its capability to detect multiple corrosions. For this purpose, the circuit was manipulated to contain several impedance mismatches at different locations representing multiple corrosions.

Figure 26 represents block diagram of the system with corrosion planted at two locations, 25km and 75km. Two mismatched impedances Z_{m1} and Z_{m2}, each 50Ω, were used to represent them. All other setting and parameters have been unchanged from the previous circuit used for single corrosion detection. The circuit was simulated and the result is shown in figure 27.

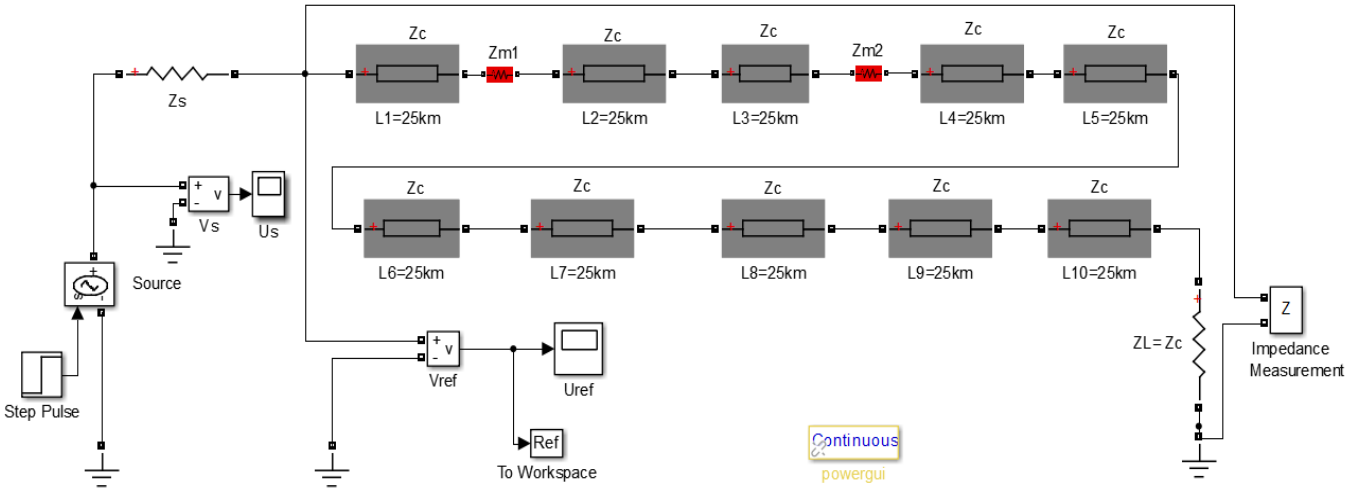

Figure 26: Corrosion at two points

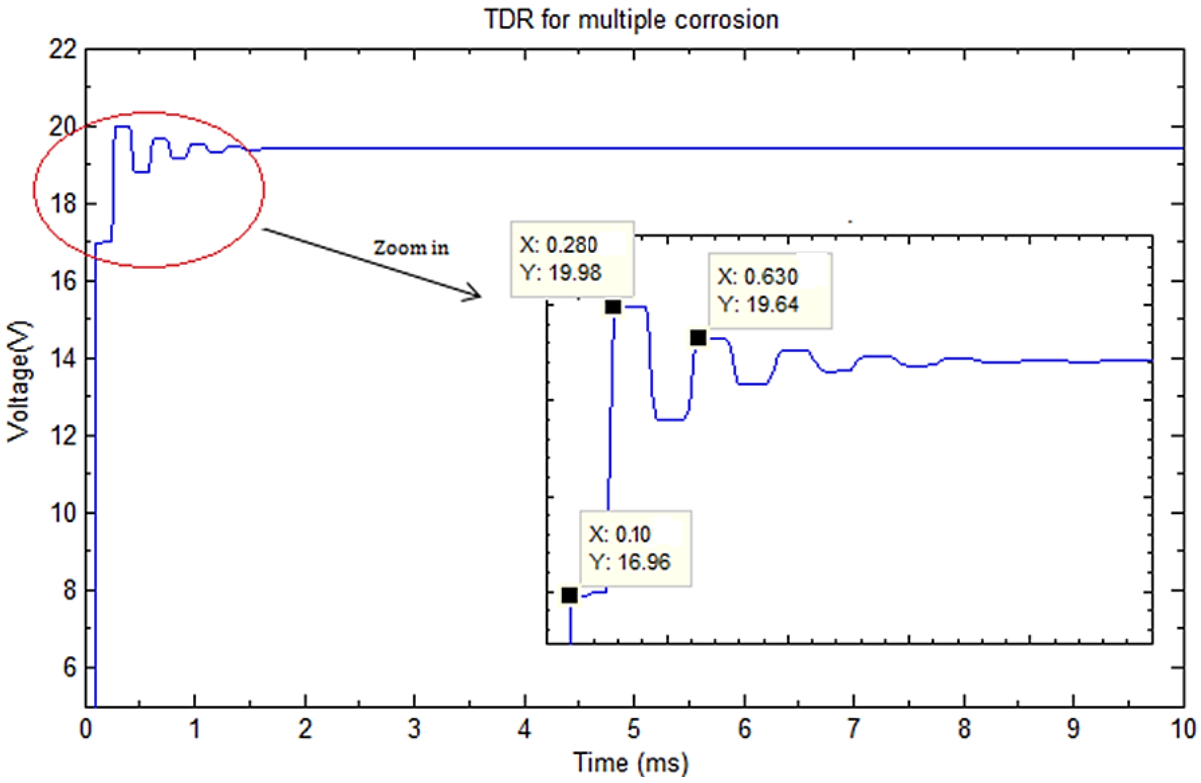

Figure 27: TDR Result for multiple corrosion at two points

In figure 27 the reflections at two points of time are shown. After the step time of 100μs of the incident pulse, the first reflection at 280μs indicates the corrosion due to the first impedance mismatch Z_{m1} at 25km. This is the same as that detected for single corrosion at 25km in figure 22 while the second reflection at 630μs is due to the impedance mismatch Z_{m2} at 75km. Further details are given in table 3 below.

Table 3: TDR result for double faults on the line at two points

Actual Fault Location (km)	Step Time (s)	Fault Time (s)	Measured Fault Location (km)	Error (%)
25	1.00E-04	2.80E-04	26.6	6.2
75	1.00E-04	6.30E-04	78.2	4.3

The numbers in this table show that the faults at two different locations on the line have been detected successfully.

It should be noted in figure 27 that multiple reflections have been detected and displayed. These reflections do not represent any further corrosion in the line but occur due to secondary reflections within the transmission line, which was thoroughly explained in bounce diagram in section 5.3.1. In this case, several reflections are not only from line's ends but also from the planted impedances. It is also important to understand that the resulting reflection coefficients may attain negative or positive values and therefore are subtracted or added to each other or to the existing signal. This may and probably will lead to cancellation of some signal reflections, and therefore, one can end up with inaccurate localization or even no detection.

In order to further investigate this process, the number of mismatch impedances is increased stepwise and the results are shown in the following figures.

As shown in figure 28, three points on the line are set corroded which are represented by Z_{m1}, Z_{m2} and Z_{m3}, at 25km, 75km and 200km respectively.

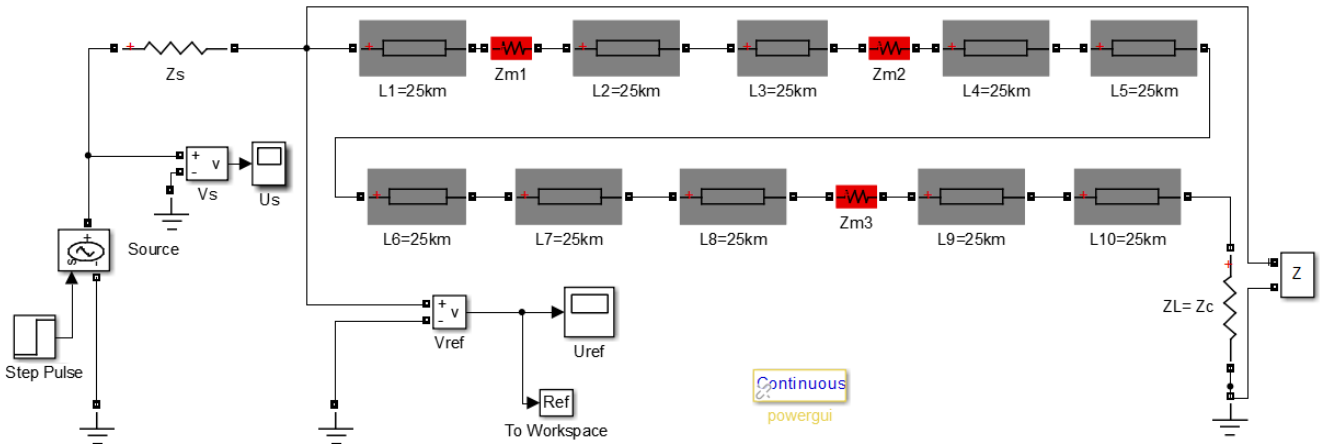

Figure 28: Multiple corrosion at three points

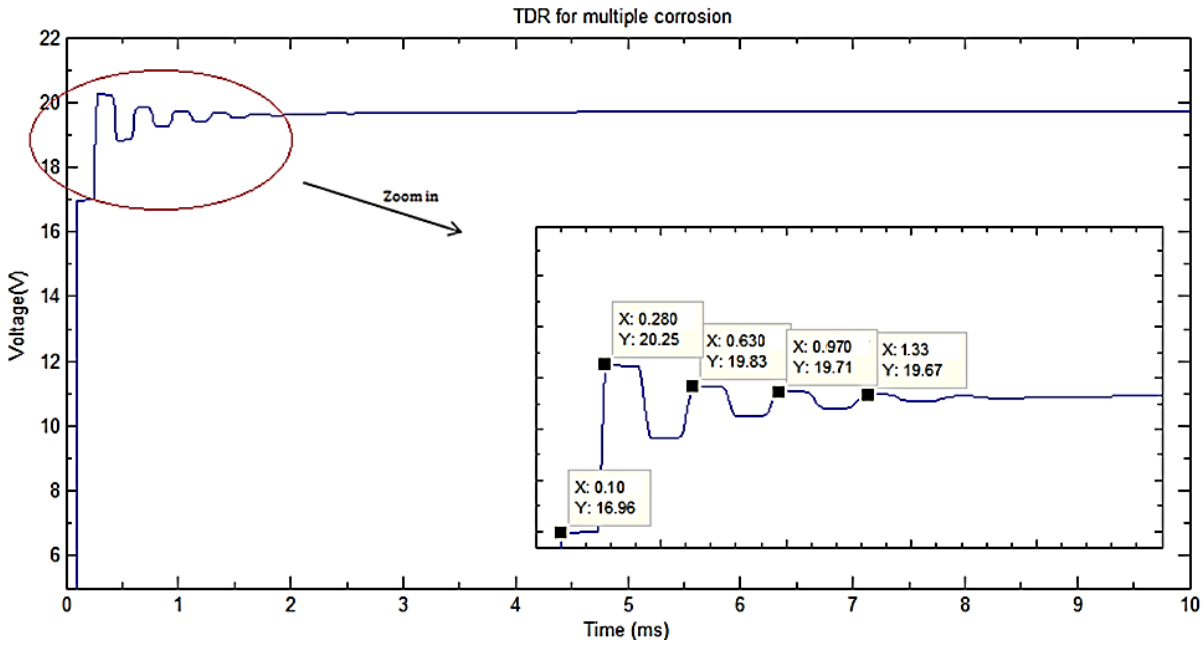

Figure 29: TDR Result for multiple corrosion at three points

According to TDR analysis, figure 29 displays a number of reflections that can lead to localization of corrosion. The first two reflections detected at 280μs and 630μs represent the corrosion at 25km and 75km respectively, similar to findings in figure 27. The reflection at 1.33ms is due to the corrosion at 200km as calculated in table 4.

Table 4: TDR result for multiple faults on the line at three points

Actual Fault Location (km)	Step Time s)	Fault Time (s)	Measured Fault Location (km)	Error (%)
25	1.00E-04	2.80E-04	26.6	6.2
75	1.00E-04	6.30E-04	78.2	4.3
200	1.00E-04	1.33E-03	181.4	9.3

Table 4 shows that TDR analysis was able to estimate the location of corrosion at three planted points. However, a combination of three mismatch impedances in this case led to an increase in the percentage error of up to 9.3%

Furthermore, a surplus reflection is pointed out at 970μs on the graph. If the location for this reflection is calculated, it yields:

$$d = 2.95 \times 10^5 \frac{(0.97 - 0.1) \times 10^{-3}}{2} = 128km$$

This location of 128km does not correspond to any mismatch impedance in the circuit of figure 28. As discussed earlier, such variations occur due to the bouncing effect of the signal in the system and can be misleading if not considered carefully.

In the next step, as shown in figure 30, four different points on the line were set corroded which are represented by Z_{m1}, Z_{m2}, Z_{m3} and Z_{m4}, at 25km, 50km, 75km and 200km respectively.

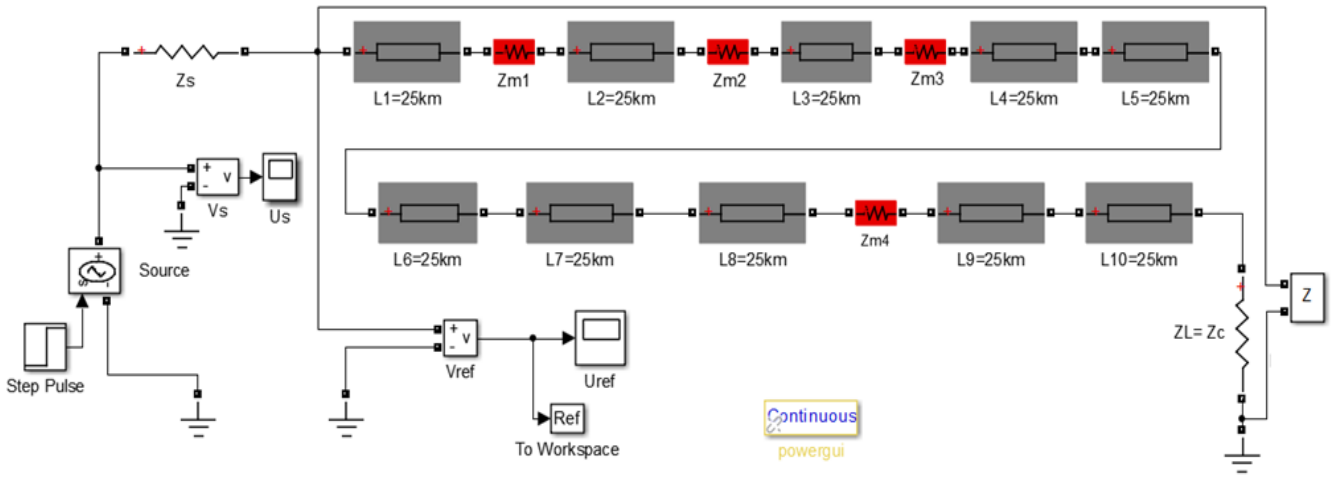

Figure 30 : Multiple corrosion at four points

The result is shown in figure 31 below. The simulation of the circuit with a combination of four mismatch impedances, in this case results in detection of only two corroded segments i.e. 25km and 75km, while the other two faults at 50km and 200km are not localized. Again a surplus reflection is pointed out at 960μs on the graph which represents a point at a distance of 127km on the line and does not correspond to any impedance mismatch.

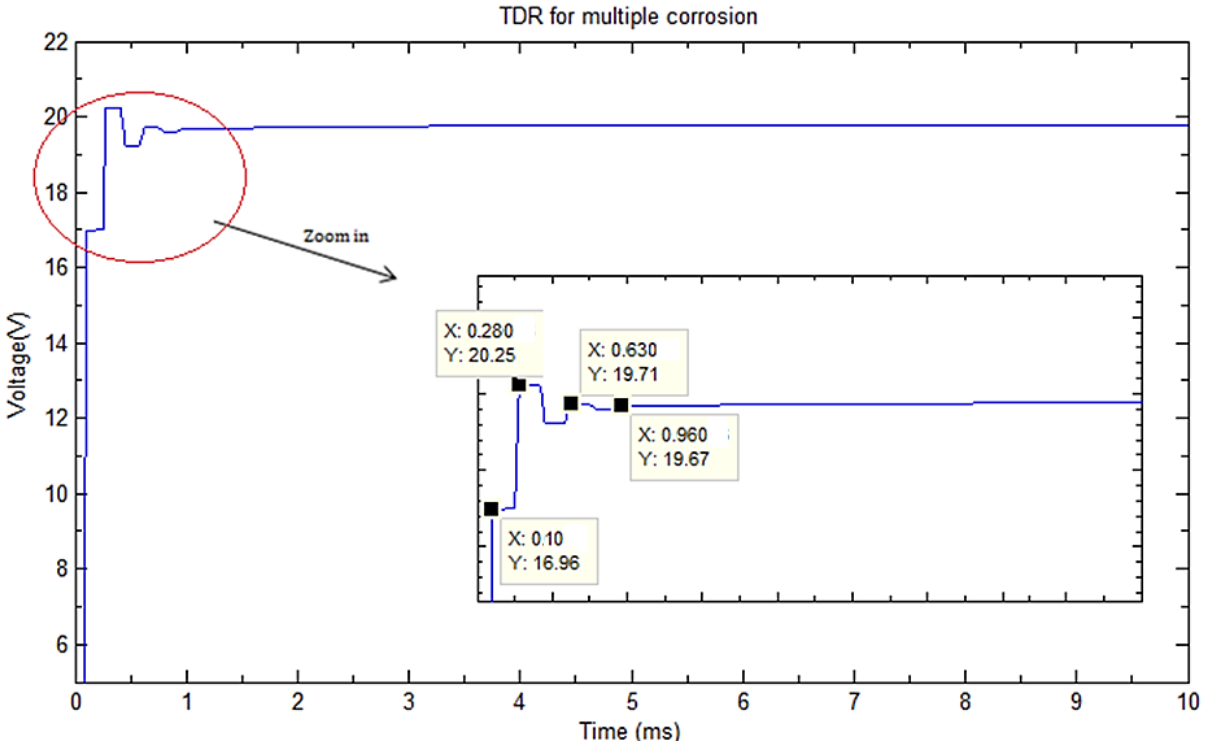

Figure 31: TDR Result for multiple corrosion at four points

Further detail is given in table 5.

Table 5: TDR result for corrosion at four points on the line

Actual Fault Location (km)	Step Time (s)	Fault Time (s)	Measured Fault Location (km)	Error (%)
25	1.00E-04	2.80E-04	26.6	6.2
50	1.00E-04	undetected	undetected	N.A.
75	1.00E-04	6.30E-04	78.2	4.3
200	1.00E-04	undetected	undetected	N.A.

In the block diagram of the circuit in figure 32, five different points on the line are set corroded which are represented by Z_{m1}, Z_{m2}, Z_{m3}, Z_{m4} and Z_{m5}, at 25km, 50km, 75km, 175km and 200km respectively.

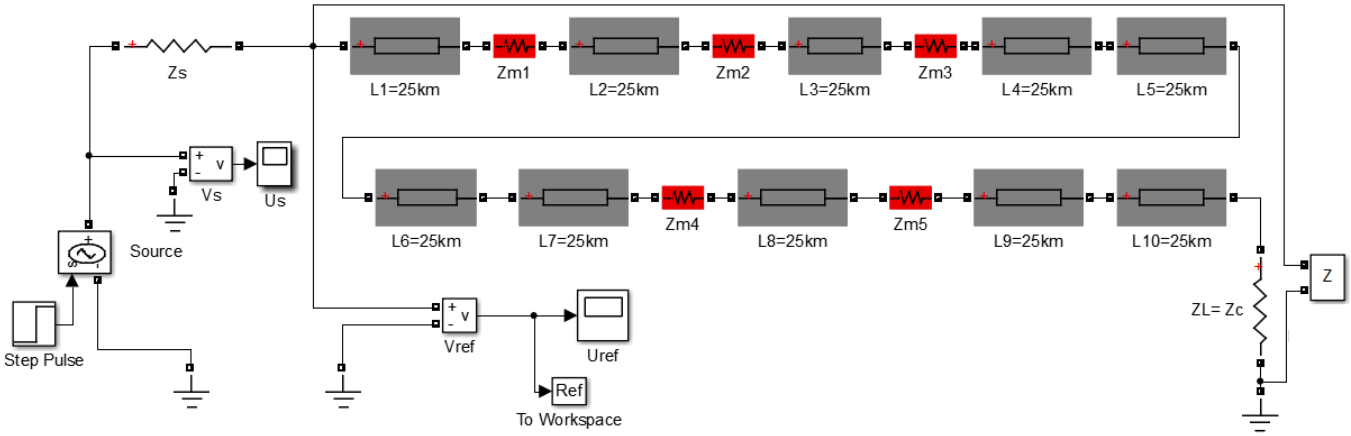

Figure 32: Multiple corrosion at five points

The simulation of the circuit with combination of five mismatch impedances in this case results in detection of only two corroded points i.e. at 25km and at 75km, while the other three faults at 50km, 175km and 200km are not localized. Moreover, the

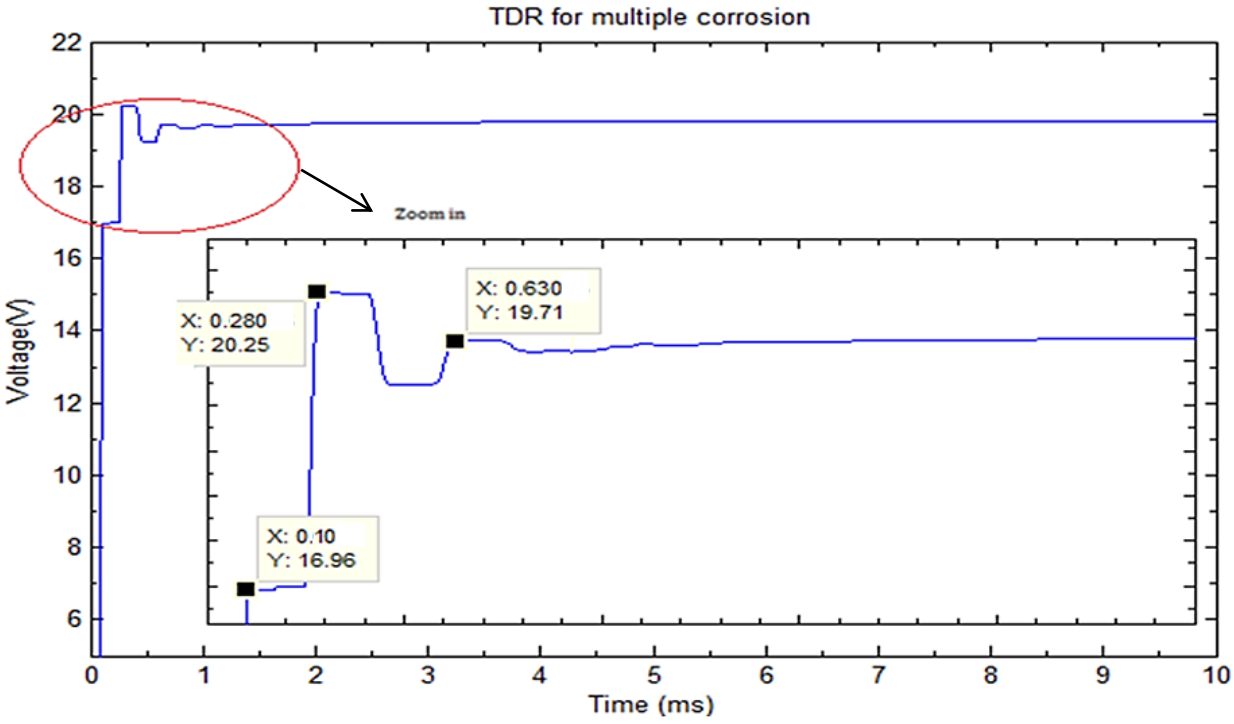

Figure 33: TDR Result for multiple corrosion at five points

interaction of multiple negative and positive waveforms ended up in cancellation of reflections and the circuit was unable to detect all the impedance mismatches.

Table 6: TDR result for multiple corrosion at five points

Actual Fault Location (km)	Step Time (s)	Fault Time (s)	Measured Fault Location (km)	Error (%)
25	1.00E-04	2.80E-04	26.6	6.2
50	1.00E-04	undetected	undetected	N.A.
75	1.00E-04	6.30E-04	78.2	4.3
175	1.00E-04	undetected	undetected	N.A.
200	1.00E-04	undetected	undetected	N.A.

It is noticed that the introduction of multiple corrosion on the transmission line decreases the capability of the circuit to detect respective impedance mismatches. At some stage it affected the accuracy of the technique by increasing the percentage error. Consequently, it is decided that the precision of TDR analysis decreases with the increase in number of mismatched impedances. In some cases a TDR result of a circuit with multiple corrosion (like in figure 33) may be easily misjudged for a circuit of fewer corrosion or even single corrosion. Therefore, it requires more experience and care when investigating a system by TDR technology. As a rule of thumb, the longer the length of the transmission line, the more is the chance of higher number of corroded points on it and vice versa. Therefore, it would be advantageous to run the test on shorter segments along the line instead of examining the whole length of the line at once.

It is also worth mentioning that there are numerous discontinuities like connectors, spacers, dampers etc. along transmission line conductors that can cause greater irregularities in the signal than that of a corroded or damaged strand at a particular location [9]. Therefore, the engineer should keep all these factors in mind before using TDR method of corrosion detection on a transmission line.

Chapter 8

- Conclusion
- Future Work Recommendation

Chapter 8: Conclusion and Future Recommendation

8.1 Conclusion

In this project, various techniques of corrosion detection in ACSR conductors of power transmission line were introduced and discussed.

The research showed that detectors based on electromagnetic induction technology can detect corrosion in steel strands as well as any flaw on aluminium strands. These detectors can identify flaws on a conductor well before other non-destructive tests could do. This method of corrosion detection is a promising technology and specialized in corrosion detection in ACSR conductors. Furthermore, the detectors not only operate on dead lines of any size but also on live lines of up to 500kV. The technology is highly sensitive, applicable, and feasible with ease of use compared to other technologies available. It has been used by companies around the globe successfully and is growing fast due to the high demand in power transmission industry. In this project, some popular detectors and their functionality were discussed.

Time domain reflectometry is a non-destructive pulse-echo technique used for the detection of faults in transmission lines. It operates on the principle of measuring reflections caused by discontinuities along a transmission line. Reflections from typical load terminations such as open circuit, short circuit and matched impedance

were discussed and their respective waveforms were shown. Essentially, the transient behaviour of the transmission line was investigated and demonstrated on bounce diagrams. It is very important to have an idea of how multiple reflections occur prior to working on TDR technique.

For the purpose of corrosion detection by the TDR method, a transmission line of 250km composed of bundled ACSR conductor with characteristic impedance of 277Ω and propagation velocity of 2.95×10^5km/s was put under investigation. This system was then imported into SimPowerSystems toolbox for modelling and simulation purposes.

The simulation outcome proved that, using TDR method, the circuit was able to detect and locate any single point corrosion along the line with an average error of less than 4%. Later, the circuit was tested for its capability of detecting multiple corrosions. Two mismatched impedances were planted in the circuit for which the result showed successful detection and localization of corrosion. When the circuit was modified for three mismatched impedances, the simulation graph still detected reflections for each location; however, this was done at the cost of increase in percentage error to 9.3%. Similarly, the circuit was modified to enclose four and then five mismatches impedances. The results showed that the circuit was unable to display reflection for each corroded locations, while some reflections represented normal locations on the line. This is concluded to be the cause of multiple bouncing effect of the signal and the interaction of positive and negative reflections that ended up to cancel or even create the appearance of surplus reflections on the signal. Therefore, the existence of multiple corrosion on transmission lines causes degradation of measurement accuracy and hence decreases the capability of the technique to function properly and sufficiently.

Overall, TDR is an effective method to obtain a general indication of the condition of a cable in a transmission line, or at least an indication of the comparative condition of two similar cables. However, there is some doubt that the technology would be operative at finding in-depth damage to conductors, such as marginally corroded strands at a particular location. This is due to the fact that corrosion at very early

stages imposes relatively small impedance change and the corresponding reflections may be undetectable. Also, there are numerous discontinuities like connectors, spacers, dampers etc. along transmission line conductors that can cause greater irregularities in the signal than that of a corroded or damaged strand at a particular location.

8.2 Future Work Recommendation

This project was mainly based on a theoretical study and computer simulation with no actual physical experiment conducted on ACSR cables or any overhead transmission lines. As the conductor deterioration due to corrosion usually leads to expensive failures and line outages, there is value in exploring technologies in this field. Recommendations in this regard would be:

1) To get a small piece of ACSR cable and measure its parameters, rather than calculation based parameters. OR

2) To obtain a piece of corroded cable and conduct TDR experiment to confirm the competency of the technology in real-world situation. It would be better to have a longer length of cable (minimum of 10m for a lab experiment) for a larger propagation time which helps in analysis in time domain observation.

3) To examine the effect of TDR on the cable having connectors or other discontinuities in order to distinguish their effect.

4) If possible, arrange for experiments to be done in coordination with a transmission or distribution company to conduct in situ investigation.

5) As was seen in this report the eddy current method is more specific in early stage corrosion detection, so it would be worth to conduct an experiment analysing this technology.

Appendices

Appendix A

Calculation of Inductance and Capacitance and Characteristic Impedance

For the purpose of calculation of line parameters, the conductor "Hare" is chosen randomly from the data sheet of General Cable in appendix B.

Inductance:

The inductance per phase per kilometre length of the transmission line under study given in figure 17 can be found using:

$$\mathrm{L} = 0.2 \ln \frac{D_{eq}}{D_{SL}} \quad \frac{\mathrm{mH}}{\mathrm{km}}$$

$$\mathrm{D_{eq}} = \sqrt[3]{\mathrm{Dab} * \mathrm{Dbc} * \mathrm{Dac}} = \sqrt[3]{4\mathrm{m} * 4\mathrm{m} * 8\mathrm{m}}$$

$$\mathrm{D_{eq}} = 5.04\mathrm{m}$$

$$\mathrm{D_{SL}} = \sqrt{\mathrm{Ds} * \mathbf{d}}$$

Where **d** is the spacing between the sub-conductors in each phase.

$$\mathrm{D_s} = 0.768\mathrm{r} = 0.768\ (7.1 \times 10^{-3} m)$$

$$\mathrm{D_s} = 5.453 \times 10^{-3} m$$

Where $\mathrm{r} = \frac{14.2}{2} \times 10^{-3} m$ radius of the conductor taken from General Cable data sheet in appendix B.

So,

$$\mathrm{D_{SL}} = \sqrt{5.453 \times 0.4 \times 10^{-3}}$$

$$\mathrm{D_{SL}} = 4.67 \times 10^{-2}\ \mathrm{m}$$

Hence,

$$\mathrm{L} = 0.2 \ln \frac{5.04}{4.67 \times 10^{-2}}$$

$$L = 0.94 \ \frac{\mathrm{mH}}{\mathrm{km}}$$

Capacitance:

In order to find the capacitance per phase for a three-phase transposed line with two-conductor bundle, the same steps are followed as the procedure for the inductance above. The capacitance per phase per unit length of the transmission line is calculated as follow [17]:

$$C = \frac{2\pi\mathcal{E}o}{ln(\frac{Deq}{D_{SC}})} \frac{F}{m}$$

$$\mathcal{E}o = 8.854 \times 10^{-12} F/m$$

$$\mathrm{D_{eq}} = \sqrt[3]{\mathrm{Dab} * \mathrm{Dbc} * \mathrm{Dac}}$$

$$= \sqrt[3]{4\mathrm{m} * 4\mathrm{m} * 8\mathrm{m}}$$

$$\mathrm{D_{eq}} = 5.04m$$

$$D_{SC} = \sqrt{\mathrm{r} * \mathbf{d}} = \sqrt{7.1 \times 10^{-3} \times 0.4}$$

$$D_{SC} = 5.33 \times 10^{-2} \ m$$

Hence,

$$C = 1.22 \ \times 10^{-11} \frac{F}{m}$$

$$C = 12.2 \ (\frac{nF}{km})$$

Characteristic Impedance

Assuming a lossless transmission line, the characteristic impedance of the line is approximated by

$$Zc = \sqrt{\frac{L}{C}}$$

$$Zc = \sqrt{\frac{0.94 \times 10^{-3}}{12.2 \times 10^{-9}}}$$

$$Zc = \sqrt{\frac{0.94 \times 10^{-3}}{12.2 \times 10^{-9}}}$$

$$Zc = 277\ \Omega$$

Appendix B

General Cable

ENERGY CABLES

ACSR

CODE NAME	ITEM NUMBER	CONDUCTOR			NOMINAL OVERALL DIAMETER	APPROX. MASS
		ALUMINIUM		STEEL		
		AREA mm²	No./mm	No./mm	mm	kg/km
HARE	66770000	105	6/4.72	1/4.72	14.2	430
DOG	66560000	105	6/4.72	7/1.57	14.2	400

TECHNICAL SPECIFICATIONS – Continued

CONDUCTOR CODE NAME	ELECTRICAL CHARACTERISTICS							
	EQUIVALENT ELECTRICAL AREAS		MAXIMUM DC RESISTANCE @20°C Ω/km	MAXIMUM AC RESISTANCE @75°C Ω/km	CURRENT RATINGS @ 75°C (a)		INDUCTIVE REACTANCE TO 0.4M Ω/km	SINGLE PHASE VOLTAGE DROP @ 0.4MSPACING MV/A.m
	ALUMINIUM mm²	COPPER mm²			WINTER NIGHT A	SUMMER NOON A		
HARE	105	64	0.273	0.330	455	334	0.276	0.86
DOG	105	64	0.273	0.330	455	334	0.276	0.86

CONDUCTOR CODE NAME	PHYSICAL PROPERTIES					
	NOMINAL OVERALL DIAMETER mm	TOTAL CROSS SECTIONAL AREA mm²	CALCULATED MINIMUM BREAKING LOAD kN	APPROX. MASS kg/km	FINAL MODULUS OF ELASTICITY GPa	COEFFICIENT OF LINEAR EXPANSION /° x 10^{-6}
HARE	14.2	122.5	36.0	430	79	19.1
DOG	14.2	118.5	32.7	390	76	19.8

Figure 34: ACSR Cable specifications [16]

Appendix C

Nominal π −model

For a transmission line, half of the shunt capacitance may be considered to be lumped at each end of the line. This is known as nominal π −model

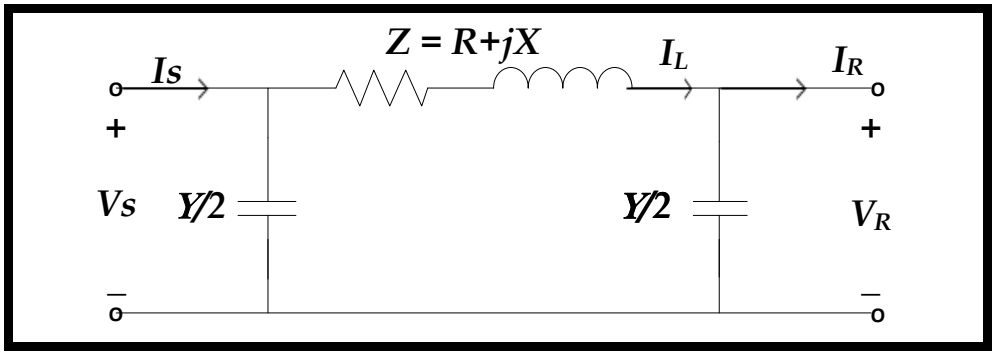

Figure 35: Nominal π-model [49]

Applying KCL and KVL:

$$I_L = I_R + \frac{Y}{2}V_R$$

$$V_S = V_R + ZI_L$$

$$V_S = V_R + Z\left(I_R + \frac{Y}{2}V_R\right)$$

$$\boldsymbol{V_S = V_R\left(1 + \frac{ZY}{2}\right) + ZI_R}$$

Also,

$$I_s = I_L + \frac{Y}{2}V_s$$

Substituting values of $I_L and\ V_s$

$$I_s = I_R + \frac{Y}{2}V_R + \frac{Y}{2}\left(V_R\left(1 + \frac{ZY}{2}\right) + ZI_R\right)$$

$$I_s = V_R \frac{Y}{2} + V_R \left(1 + \frac{ZY}{2}\right) \frac{Y}{2} + I_R + Z I_R \frac{Y}{2}$$

$$I_s = V_R \frac{Y}{2} \left(2 + \frac{ZY}{2}\right) + I_R \left(1 + \frac{ZY}{2}\right)$$

$$\boldsymbol{I_s = V_R Y \left(1 + \frac{ZY}{4}\right) + I_R \left(1 + \frac{ZY}{2}\right)}$$

Appendix D

Derivation of Equations for Transmission Line Model

Consider the circuit in figure 7. The transmission line equations can be obtained by applying Kirchhoff's voltage and current laws to the circuit above [49]. Considering a small section of line Δx at a distance x from the receiving end of the line, the phasor voltages on both sides of this segment are

$$\mathrm{V(x + \Delta x) = V(x) + z\,\Delta x\, I(x)}$$

Rearranging,

$$\frac{\mathrm{V(x + \Delta x) - V(x)}}{\mathrm{\Delta x}} = \mathrm{z\, I(x)} \quad ----------(21)$$

From the definition of limit, when $\mathrm{\Delta x \to 0}$

$$\frac{\mathrm{dV(x)}}{\mathrm{dx}} = \mathrm{z\, I(x)} \quad ----------(22)$$

Similarly, the phasor current is:

$$\mathrm{I(x + \Delta x) = I(x) + y\,\Delta x\, V(x + \Delta x)}$$

Rearranging,

$$\frac{\mathrm{I(x + \Delta x) - I(x)}}{\mathrm{\Delta x}} = \mathrm{y\, V(x + \Delta x)} \quad ----------(23)$$

Again, taking limit as $\Delta x \to 0$

$$\frac{dI(x)}{dx} = y\,V(x) \qquad ---------- (24)$$

Differentiating equation (22):

$$\frac{d^2V(x)}{dx^2} = z\,\frac{dI(x)}{dx} \qquad ---------- (25)$$

Substituting equation (24) in equation (25):

$$\frac{d^2V(x)}{dx^2} = z\,y\,V(x) \qquad ---------- (26)$$

Let

$$\gamma^2 = zy ---------- (27)$$

So we are left with the second order differential equation:

$$\frac{d^2V(x)}{dx^2} = \gamma^2\,V(x)$$

Or

$$\frac{d^2V(x)}{dx^2} - \gamma^2 V(x) = 0$$

The solution of this second order equation is:

$$V(x) = K_1 e^{\gamma x} + K_2 e^{-\gamma x} \qquad ---------- (28)$$

Where γ known as the propagation constant is a complex expression given by:

$$\gamma = \alpha + j\beta \qquad ---------- (29)$$

The real part α is called the attenuation constant and the imaginary part β is known as the phase constant.

From equation (27)

$$\gamma = \alpha + j\beta = \sqrt{zy} = \sqrt{(R + jwL)(G + jwC)} \quad ----------(30)$$

Differentiating equation (28) with respect to x

$$\frac{dV(x)}{dx} = \gamma(K_1 e^{\gamma x} - K_2 e^{-\gamma x})$$

Comparing this with equation (22)

$$z\, I(x) = \gamma(K_1 e^{\gamma x} - K_2 e^{-\gamma x})$$

$$I(x) = \frac{\sqrt{zy}}{z}(K_1 e^{\gamma x} - K_2 e^{-\gamma x}) \qquad \because \gamma = \sqrt{zy}$$

$$I(x) = \sqrt{\frac{y}{z}}(K_1 e^{\gamma x} - K_2 e^{-\gamma x})$$

$$I(x) = \frac{1}{Z_c}(K_1 e^{\gamma x} - K_2 e^{-\gamma x}) \quad ----------(31)$$

Where $Z_c = \sqrt{\frac{z}{y}} = \sqrt{\frac{r+jwL}{g+jwC}}$ is known as the characteristic impedance.

In order to find the constants K_1 *and* K_2 we note that when $x = 0$, $V(x) = V_R$, and $I(x) = I_R$

Equation (28) becomes:

$$V_R = K_1 e^0 + K_2 e^0 = K_1 + K_2 \quad ----------(32)$$

Similarly, from (31):

$$I_R = \frac{1}{Zc}(K_1 - K_2)$$

$$I_R Zc = (K_1 - K_2) ----------(33)$$

Adding equations (32) and (33), we get:

$$V_R + I_R Zc = 2K_1$$

$$K_1 = \frac{V_R + I_R Z_c}{2} \quad ---------- (34)$$

Similarly, subtracting equations (33) from (33), we get:

$$K_2 = \frac{V_R - I_R Z_c}{2} \quad ---------- (35)$$

Substituting these values of constants back in equation (28) and (31), we can get general expressions representing voltage and current along the transmission line.

$$V(x) = \frac{V_R + I_R Z_c}{2} e^{\gamma x} + \frac{V_R - I_R Z_c}{2} e^{-\gamma x}$$

$$V(x) = \frac{e^{\gamma x} + e^{-\gamma x}}{2} V_R + Z_c \frac{e^{\gamma x} - e^{-\gamma x}}{2} I_R \quad ----------(36)$$

And,

$$I(x) = \frac{1}{Z_c}\left(\frac{V_R + I_R Z_c}{2} e^{\gamma x} - \frac{V_R - I_R Z_c}{2} e^{-\gamma x}\right)$$

$$I(x) = \frac{1}{Z_c}\frac{e^{\gamma x} - e^{-\gamma x}}{2} V_R + \frac{e^{\gamma x} + e^{-\gamma x}}{2} I_R \quad ---------- (37)$$

From the hyperbolic functions:

$$\sinh \gamma x = \frac{e^{\gamma x} - e^{-\gamma x}}{2}$$

$$\cosh \gamma x = \frac{e^{\gamma x} + e^{-\gamma x}}{2}$$

Hence, equation (36) and (37) become:

$$V(x) = \cosh \gamma x \, V_R + Zc \sinh \gamma x \, I_R \quad ----------(38)$$

$$I(x) = \frac{1}{Z_c} \sinh \gamma x \, V_R + \cosh \gamma x \, I_R \quad ---------- (39)$$

We can find a relation between the two ends of the line by setting *x=l, V(l)=V(s) and I(l)= I(s),*

$$V(s) = \cosh \gamma l \, V_R + Z_c \sinh \gamma l \, I_R \quad ----------(40)$$

$$I(s) = \frac{1}{Z_c} \sinh \gamma l \, V_R + \cosh \gamma l \, I_R \quad ----------(41)$$

Re-writing these equations for ABCD constants

$$\begin{bmatrix} V_s \\ I_s \end{bmatrix} = \begin{bmatrix} A & B \\ C & D \end{bmatrix} \begin{bmatrix} V_R \\ I_R \end{bmatrix}$$

Where,

$$\mathbf{A} = \boldsymbol{cosh}\ \boldsymbol{\gamma l} \qquad \mathbf{B} = \mathbf{Z_c}\ \boldsymbol{sinh}\ \boldsymbol{\gamma l}$$

$$\boldsymbol{C} = \frac{\mathbf{1}}{\mathbf{Z_c}}\boldsymbol{sinh}\ \boldsymbol{\gamma l} \qquad \boldsymbol{D} = \mathbf{A} = \boldsymbol{cosh}\ \boldsymbol{\gamma l}$$

It can be seen that

AD - BC = 1

$$cosh^2 \gamma l - (Z_c \, sinh \, \gamma l)\frac{1}{Z_c} sinh \, \gamma l = cosh^2 \gamma l - sinh^2 \gamma l = 1$$

We can replace the ABCD constants in the equivalent π −model shown in figure 35.

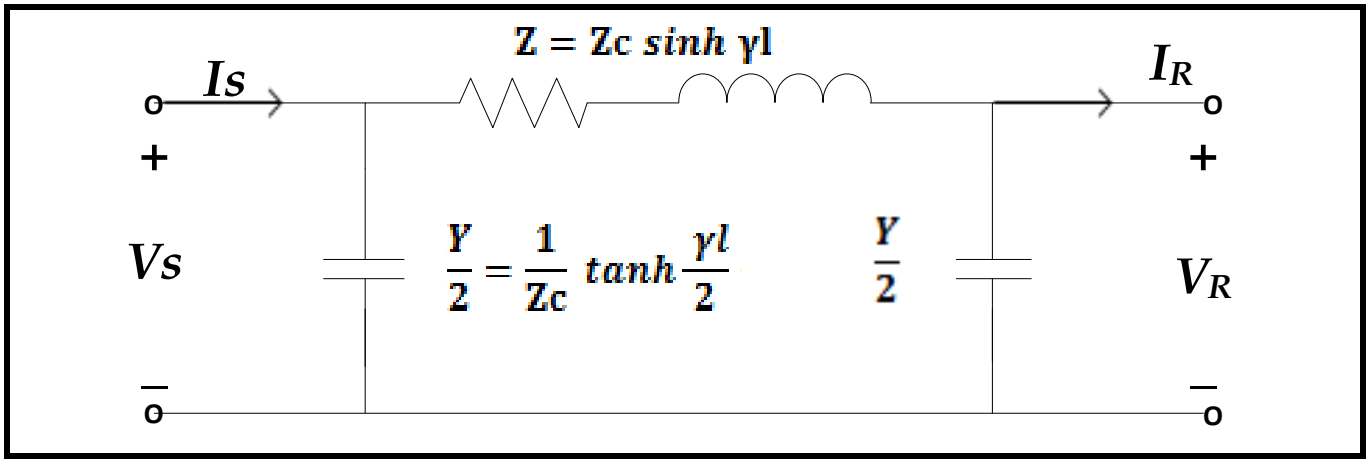

Figure 36: Equivalent π-model [49]

The expressions for this equivalent π −model are as follow:

$$V(s) = V_R\left(1+\frac{ZY}{2}\right) + Z\,I_R \quad ----------(42)$$

$$I_s = V_R Y\left(1+\frac{ZY}{4}\right) + I_R\left(1+\frac{ZY}{2}\right) \quad ----------(43)$$

Comparing equation (42) with (40)

$$\mathbf{Z = Z_c}\ \boldsymbol{sinh}\ \boldsymbol{\gamma l} \quad ----------(44)$$

The comparison also gives,

$$cosh\ \gamma l = (1+\frac{ZY}{2})$$

$$\frac{ZY}{2} = cosh\ \gamma l - 1 \quad ----------(45)$$

Dividing equation (45) by (44) and using the identity $tanh\frac{n}{2} = \frac{cosh\ n-1}{sinh\ n}$

$$\frac{cosh\ \gamma l - 1}{Z_c\ sinh\ \gamma l} = \frac{\frac{ZY}{2}}{Z}$$

$$\frac{1}{Z_c}\ tanh\frac{\gamma l}{2} = \frac{Y}{2} \qquad \because Z_c = \sqrt{\frac{z}{y}}$$

$$\mathbf{\frac{Y}{2} = \frac{1}{Z_c}\ tanh\frac{\gamma l}{2}} \quad ----------(46)$$

References:

[1]. Advanced Technology Testing and Research. ATTAR. 2013. Available online at: http://www.attar.com.au/overhead-line-corrosion-detection.aspx (accessed 11/05/2013).

[2]. Aggarwal, R. K., A. T. Johns, J. A. S. B. Jayasinghe, and W. Su. 2000. "An overview of the condition monitoring of overhead lines." *Electric Power Systems Research* no. 53 (1):15-22. doi: http://dx.doi.org/10.1016/S0378-7796(99)00037-1.

[3]. Baltazar, A., C. D. Hernandez-Salazar, and B. Manzanares-Martinez. 2010. "Study of wave propagation in a multiwire cable to determine structural damage." Ndt & E International no. 43 (8):726-732. doi: 10.1016/j.ndteint.2010.08.007.

[4]. Bayliss, C. R., and B. J. Hardy. 2012. Transmission and distribution electrical engineering. Oxford: Newnes. Access Online via Elsevier.

[5]. Cheng, D.K. 1989. *Field and Wave Electromagnetic*. 2nd ed: Addison Wesley Publishing Company.

[6]. Cormon. A Teledyne Technologies Company. 2013. Available online at: http://www.cormon.com/products/datasheets%5Cptp002.pdf accessed on 10/10/2013

[7]. da Frota MOREIRA, Pedro L, Plutarcho M LOURENCO, Av Horacio de Macedo CEPEL, Celia Regina SH LOURENCO, Mauro Zanini SEBRAO, SANT'ANNA Ildejairo, and Jose Felipe AG WAVRIK. 2008. "Internal Corrosion in Conductor Cables of Power Transmission Lines: Characterization of the Atmosphere and Techniques for Faults Detection."

[8]. Dewart.com. online at: http://www.dewart.com/ accessed on: 05/11/2013

[9]. Electric Power Research Institute. 2000. "Inspection & Assessment of Overhead Line Conductors." A State-of-the-Science Report. Palo Alto. CA: 1000258.

[10]. Enokizono, M., and S. Nagata. 1992. "Non-Destructive Testing with Magnetic Sensor Using Rotational Magnetic Flux." *Magnetics in Japan, IEEE Translation Journal on* no. 7 (3):241-249. doi: 10.1109/TJMJ.1992.4565368.

[11]. Ferguson, J. M., and R. R. Gibbon. 1994. "Overhead transmission lines-refurbishment and developments." *Power Engineering Journal* no. 8 (3):109-118. doi: 10.1049/pe:19940303.

[12]. Findlay, Raymond D., and G. Pandurangan. 1970. "A Comparison Between Two Different Designs of Bare Single-Layer Steel-Reinforced Aluminum Conductor." *Power*

Apparatus and Systems, IEEE Transactions on no. PAS-89 (7):1470-1474. doi: 10.1109/TPAS.1970.292578.

[13]. Fisher, S.A., I. R. Funnel, and S.T. Larsen. 1989. The Detection of Overhead Line Conductor Damage by Helicopter Borne Thermal Images, Sixth International Symposium on High Voltage Engineering, New Orleans.

[14]. Flicker.com [online]. http://www.flickr.com/photos/8755091@N07/7240603688 accessed on: 05/11/2013

[15]. Fujikura. Fujikura News. 07 2012. [online]. http://www.fujikura.co.jp/ng/f-news/372.pdf (accessed 11 02, 2013).

[16]. General Cable. 2013. Energy Cables ACSR. Available online. Retrieved from: http://www.generalcable.com.au/getattachment/7046493c-989c-418e-8735-ea3642d20082 Accessed on 28/09/2013. Accessed on 28/09/2013

[17]. Glover, J. D., Sarma, M. S. and T. J. Overbye. 2011. Power system analysis and design. 5th ed. Stamford, CT : Cengage Learning.

[18]. Greenfield, E. W., and E. W. Everhart. 1957. "A Field Study of Acsr Cable in Severe Marine and Industrial Environment." Power apparatus and systems, part iii. transactions of the american institute of electrical engineers no. 76 (3):106-117. doi: 10.1109/AIEEPAS.1957.4499512.

[19]. Guntner, O., L. Schmidt, L. Varga, S. Simon, and J. Szabo. 1999. Corrosion detector for assessing the remaining life of old steel reinforced aluminium conductors. Paper read at Electric Power Engineering, 1999. PowerTech Budapest 99. International Conference on, Aug. 29 1999-Sept. 2 1999.

[20]. Guru, B. S. and H. R. Hızıroğlu. 2004.Electromagnetic field theory fundamentals 2nd ed. Cambridge University Press, Cambridge, UK ; New York.

[21]. Hambley, A. R. 2008. Electrical engineering: principles and applications: Pearson Prentice Hall.

[22]. Hansen, J. 2004. "The Eddy current inspection method, Part 1 – History and electrical theory", Insight Vol 46 No. 5, May/2004, pp 279 - 281.

[23]. Hartebrodt, M., and K. Kabitzsch. 2004. Fault detection in fieldbuses with time domain reflectometry.

[24]. Harvard, D. G., G. Bellamy, P. G. Buchan, H. A. Ewing, D. J. Horrocks, S. G. Krishnasamy, J. Motlis, and K. S. Yoshiki-Gravelsins. 1992. "Aged ACSR conductors. I. Testing procedures for conductors and line items." *Power Delivery, IEEE Transactions on* no. 7 (2):581-587. doi: 10.1109/61.127052.

[25]. Hashmi, Ghulam Murtaza. 2008. *Partial discharge detection for condition monitoring of covered-conductor overhead distribution networks using Rogowski coil*: Teknillinen korkeakoulu.

[26]. Hashmi, G. M., R. Papazyan, and M. Lehtonen. 2007. Comparing Wave Propagation Characteristics of MV XLPE Cable and Covered-Conductor Overhead Line using Time Domain Reflectometry Technique. Paper read at Electrical Engineering, 2007. ICEE '07. International Conference on, 11-12 April 2007.

[27]. Havard, D. G., G. Bellamy, P. G. Buchan, H. A. Ewing, D. J. Horrocks, S. G. Krishnasamy, J. Motlis, and K. S. Yoshiki-Gravelsins. 1991. Aged ACSR conductors. I. Testing procedures for conductors and line items. Paper read at Transmission and Distribution Conference, 1991., Proceedings of the 1991 IEEE Power Engineering Society, 22-27 Sep 1991.

[28]. Hewlett-Packard.1998. Time Domain Reflectometry Theory: Hewlett-Packard Application Note 1304-2, Hewlett-Packard Company, Palo Alto, Calif.

[29]. Ivanov, Plamen Alexandrov. 2002. *Remote field eddy current probes for the detection of stress corrosion cracks in transmission pipelines*. Ph.D., Iowa State University, Ann Arbor.

[30]. Jiang, Xingliang, and Yunfeng Xia. 2010. A GA based optimized designation of detection sensor for broken steel stranded wire faults in ACSR. Paper read at High Voltage Engineering and Application (ICHVE), 2010 International Conference on, 11-14 Oct. 2010.

[31]. Jomdecha, C., and A. Prateepasen. 2009. "Design of modified electromagnetic main-flux for steel wire rope inspection." *NDT & E International* no. 42 (1):77-83. doi: http://dx.doi.org/10.1016/j.ndteint.2007.10.006.

[32]. Karabay, Sedat, and F. Kaya Önder. 2004. "An approach for analysis in refurbishment of existing conventional HV–ACSR transmission lines with AAAC." Electric Power Systems Research no. 72 (2):179-185.
doi: http://dx.doi.org/10.1016/j.epsr.2004.03.014

[33]. Komoda, M., T. Kawashima, M. Minemura, A. Mineyama, M. Aihara, Y. Ebinuma, T. Kanno, and M. Kiuchi. 1990. "Electromagnetic induction method for detecting and locating flaws on overhead transmission lines." *Power Delivery, IEEE Transactions on* no. 5 (3):1484-1490. doi: 10.1109/61.57992.

[34]. Lee, C. Q. 1987. "A Novel Approach to Transients in Transmission Lines." *Education, IEEE Transactions on* no. E-30 (2):71-76. doi: 10.1109/TE.1987.5570524.

[35]. Liu, Fang. 2006. *A study on modelling of single layer ACSR conductors*. Ph.D., McMaster University (Canada), Ann Arbor.

[36]. Liu, Wei. 2002. *Electromagnetic modeling of embedded metallic structures for nondestructive evaluation using time-domain reflectometry*. Ph.D., University of Delaware, Ann Arbor.

[37]. Liu, W., R. Hunsperger, M. Chajes, and E. Kunz. 2001. An overview of corrosion damage detection in steel bridge strands using TDR. Paper read at Proc., 2nd Int. Symp. on TDR for Innovative Applications.

[38]. Mathworks. 2013. Online: http://www.mathworks.com.au/help/physmod/sps/powersys/ref/distributedparameterline.html and http://www.mathworks.com.au/products/simpower/ Accessed on: 01/11/2013

[39]. Mayer P. 1998. Corrosion evaluation methods for power transmission lines. http://www.ams.tuke.sk/data/ams_online/1998/number3/mag08/mag08.pdf

[40]. Mamiş, Mehmet Salih, Müslüm Arkan, and Cemal Keleş. 2013. "Transmission lines fault location using transient signal spectrum." *International Journal of Electrical Power & Energy Systems* no. 53 (0):714-718. doi: http://dx.doi.org/10.1016/j.ijepes.2013.05.045.

[41]. Mijarez, R., and A. Baltazar. 2013. "GUIDED WAVE PROPAGATION STUDY IN AN ACSR CABLE WITH ARTIFICIAL DAMAGE." In *Review of Progress in Quantitative Nondestructive Evaluation, Vols 32a and 32b*, edited by D. O. Thompson and D. E. Chimenti, 1417-1424.

[42]. Mijarez, R., F. Martinez, and A. Baltazar. 2011. "REAL TIME DAMAGE DETECTION SYSTEM USING GUIDED WAVES IN ACSR CABLES." *AIP Conference Proceedings* no. 1335 (1):1402-1409.

[43]. Papazyan, R. (2005). Techniques for Localization of Insulation Degradation along Medium-Voltage Power Cables", Doctoral dissertation, The Royal Institute of Technology(KTH), Stockholm, Sweden,

[44]. Papazyan, R., and R. Eriksson. 2003. "Calibration for time domain propagation constant measurements on power cables," Instrumentation and Measurement, IEEE Transactions on, vol.52, no.2, pp.415,418.
doi: 10.1109/TIM.2003.811657

[45]. Peng, Xu, Huang Songling, and Wei Zhao. 2010. Differential eddy current testing sensor composed of double gradient winding coils for crack detection. Paper read at Sensors Applications Symposium (SAS), 2010 IEEE, 23-25 Feb. 2010.

[46]. Pinto, A. V., M. Z. Sebrao, C. R. S. H. Lourenco, I. S. de Almeida, J. Saad, and P. M. Lourenco. 2010. Remote detection of internal corrosion in conductor cables of power transmission lines. Paper read at Applied Robotics for the Power Industry (CARPI), 2010 1st International Conference on, 5-7 Oct. 2010.

[47]. Qinghai, Shi, U. Troeltzsch, and O. Kanoun. 2010. Detection and localization of cable faults by time and frequency domain measurements. Paper read at Systems Signals and Devices (SSD), 2010 7th International Multi-Conference on, 27-30 June 2010.

[48]. Rao. B.P.C. "Non-Destructive Testing".(Online). Available at: http://www.geocities.ws/raobpc/NDT.html. Access date: 02/11/2013

[49]. Saadat, H. 2002. Power System Analysis. 2nd ed. Boston: McGraw-Hill.

[50]. Sung, D. K., and M. M. Morcos. 2003. "Mechanical deterioration of ACSR conductors due to forest fires." *Power Delivery, IEEE Transactions on* no. 18 (1):271-276. doi: 10.1109/TPWRD.2002.804011.

[51]. Sutton, J., and K.G. Lewis. 1986. "The detection of internal corrosion in steel-reinforced aluminium overhead power line conductors." UK Corrosion '86. Birmingham, UK. Vol 1. 345-359.

[52]. Thayoob, Y. H. Md., A. M. Ariffin, and S. Sulaiman. 2010. Analysis of high frequency wave propagation characteristics in medium voltage XLPE cable model. Paper read at Computer Applications and Industrial Electronics (ICCAIE), 2010 International Conference on, 5-8 Dec. 2010.

[53]. Tleis, Nasser D. 2008. "3 - Modelling of multi-conductor overhead lines and cables." In *Power* Systems Modelling and Fault Analysis, 74-199. Oxford: Newnes.

[54]. Wang, J., P. E. C. Stone, Y. J. Shin, and R. A. Dougal. 2010. "Application of joint time-frequency domain reflectometry for electric power cable diagnostics." Signal Processing, IET no. 4 (4):395-405. doi: 10.1049/iet-spr.2009.0137.

[55]. Wikipedia. (2013, Oct.) [Online]. Transmission Line. http://commons.wikimedia.org/wiki/File:Pylon_ds.jpg attributed to Yummifruitbat.

[56]. Wikipedia. (2013, Oct.) [Online]. ACSR Cable. http://commons.wikimedia.org/wiki/File:ACSR_%26_ACCC_Conductors.JPG